Obtaining extended insight into molecular systems by probing multiple pathways in second-order nonlinear spectroscopy

Alexander P. Fellows ⬤ ; Vasileios Balos ⬤ ; Ben John; Álvaro Díaz Duque; Martin Wolf ⬤ ; Martin Thämer ✉

Check for updates

View Online   Export Citation   CrossMark

The Journal of Chemical Physics

AIP Publishing

Obtaining extended insight into molecular systems by probing multiple pathways in second-order nonlinear spectroscopy

View Online   Export Citation   CrossMark

Alexander P. Fellows,[1] (ID) Vasileios Balos,[1,2] (ID) Ben John,[1] Álvaro Díaz Duque,[1] Martin Wolf,[1] (ID) and Martin Thämer[1,a)]

AFFILIATIONS

[1] Fritz Haber Institute of the Max Planck Society, Faradayweg 4-6, 14195 Berlin, Germany
[2] Instituto Madrileño de Estudios Avanzados en Nanociencia (IMDEA Nanociencia), 28049 Madrid, Spain

[a)]Author to whom correspondence should be addressed: thaemer@fhi-berlin.mpg.de. **Tel:** +49 (0)30 8413 5220

ABSTRACT

Second-order nonlinear spectroscopy is becoming an increasingly important technique in the study of interfacial systems owing to its marked ability to study molecular structures and interactions. The properties of such a system under investigation are contained within their intrinsic second-order susceptibilities which are mapped onto the measured nonlinear signals (e.g. sum-frequency generation) through the applied experimental settings. Despite this yielding a plethora of information, many crucial aspects of molecular systems typically remain elusive, for example the depth distributions, molecular orientation and local dielectric properties of its constituent chromophores. Here, it is shown that this information is contained within the phase of the measured signal and, critically, can be extracted through measurement of multiple nonlinear pathways (both the sum-frequency and difference-frequency output signals). Furthermore, it is shown that this novel information can directly be correlated to the characteristic vibrational spectra, enabling a new type of advanced sample characterization and a profound analysis of interfacial molecular structures. The theory underlying the different contributions to the measured phase of distinct nonlinear pathways is derived, after which the presented phase disentanglement methodology is experimentally demonstrated for model systems of self-assembled monolayers on several metallic substrates. The obtained phases of the local fields are compared to the corresponding phases of the nonlinear Fresnel factors calculated through the commonly used theoretical model, the three-layer model. It is found that, despite its rather crude assumptions, the model yields remarkable similarity to the experimentally obtained values, thus providing validation of the model for many sample classes.

INTRODUCTION

Over the last few decades, second order vibrational spectroscopic techniques, such as sum-frequency generation (SFG) spectroscopy, have had an enormous impact on our understanding of molecular systems due to the wealth of information that they can reveal. Like their linear counterparts, these techniques can be employed to analyse microscopic structures and molecular compositions, but, due to the highly restrictive symmetry selection rules of second order nonlinear processes, important additional information can be obtained. Examples are molecular symmetry, spatial order, or molecular orientation.[1–3] It is these peculiar selection rules that also make SFG particularly useful for the study of interfacial systems. Within the electric dipole approximation, these techniques probe anisotropic environments which, for the majority of materials, are only present in interfacial regions.[4] For this reason, SFG spectroscopy has been used to make many significant advances in the

understanding of the structure and interactions at a large range of interfaces.[1,5–7]

Despite the vast range of accessible information, for a full description of a molecular system (especially at interfaces) even more important parameters are required. Additional key information includes, for example, details about the spatial (depth) distributions of its constituent chromophores, characteristics of the local dielectric environments, and, crucially, how these correlate to the other observables. Gaining access to such correlated information would open up the possibility to new types of sample studies and to a far deeper understanding of the molecular structures at interfaces. However, these parameters have so far been highly challenging to access through spectroscopic measurements, although this information is generally encoded within the measured nonlinear response, more precisely in their phases.

In second order techniques, the spectroscopic information is governed by the second order susceptibility of the system. In this context, it is important to distinguish between two types of susceptibilities, namely, the intrinsic susceptibility which is directly associated with the properties of the molecular system (and thus independent of how the sample is being probed), and the measured (effective) susceptibility which is influenced by the intrinsic response, but also contains other extrinsic (experimental) factors which can be modulated. Clear examples of this modulation are polarisation- or angular-dependent measurements which vary the contributions of different tensor components of the intrinsic susceptibility to the measured susceptibility. Such an approach is commonly exploited to obtain insight into the molecular symmetry.[1] Beyond the angular and polarisation control, permutation of the frequencies within the nonlinear light–matter interaction (probing different interaction pathways) also represents such a modulation, although it has not yet been fully exploited. In this contribution, it is shown how such a frequency permutation, through measuring both phase-sensitive SFG and difference-frequency generation (DFG) responses, can be used to precisely determine both depth distributions of the chromophores and information on their local dielectric environments.

As mentioned above the key to such information is the phase of the measured susceptibility. Explicitly, the overall phase of the measured second order response can be broken down into three contributions:

1. Firstly, the intrinsic resonant contributions of the chromophores will change phase from 0 to $\pm\pi$ (or vice versa) as the IR beam passes through the resonant frequency. Therefore, the combination of resonances within a spectral region will yield a strong contribution to the overall phase, potentially exploring the entire phase-space across the spectrum.[8] This is the phase of the intrinsic susceptibility, denoted here as $\varphi_R(\omega)$, and can be used to access the details of the molecular orientation based on the absolute sign of the phase of each resonance and the direction of the corresponding transition dipole vector.

2. Secondly, the propagation path length of the involved beams will also influence the phase of the measured signal.[9–11] This contribution to the overall phase is denoted as $\varphi_P(\omega)$ and is directly linked to the depth coordinate of the corresponding chromophore via the specific wave vector mismatch of the involved beams. Whilst this phase will continuously cycle from 0 to 2π for an isolated chromophore at increasing depths, with a distribution of chromophores following a decaying functional form the propagation phase of the integrated response is well-defined, yielding an unambiguous depth coordinate.

3. Lastly, in the presence of an absorbing material, the nonlinear Fresnel factors, which govern the local fields in the vicinity of a chromophore, will become complex and thus also contribute a phase to the overall measured susceptibility.[12] This will be denoted $\varphi_L(\omega)$ and has a frequency dependence dictated by the complex refractive index of the absorbing medium. Therefore, the relative contributions of dispersion and absorption to the local dielectric function are exactly accessible from this phase.

Therefore, the overall phase of the measured susceptibility will be constructed as in Eq. (1),

$$\varphi(\omega) = \varphi_R(\omega) + \varphi_P(\omega) + \varphi_L(\omega) \qquad (1)$$

with the first contribution representing the phase of the intrinsic susceptibility and the other two being extrinsic contributions arising from the details of experimental measurement of the chromophore(s). Although the two extrinsic contributions, $\varphi_P(\omega)$ and $\varphi_L(\omega)$, only appear due to the sample being probed and thus depend on the specific experimental settings, they obviously **report** on intrinsic properties of the system. Specifically, the depth distribution of each chromophore and local dielectric properties (which are not contained within the intrinsic susceptibility) are mapped onto the effective susceptibility through the measurement process. To make the spectroscopic information contained within these different phase contributions accessible, the sum in Eq. (1) must be decomposed. Unfortunately, such a decomposition is not generally possible solely through measuring the response from single phase-sensitive second order pathway (e.g., just SFG alone). As will be shown here, this challenge can be overcome by the combined measurement of phase-sensitive SFG and DFG as this modulates (via sign flips) the phases of the extrinsic contributions, $\varphi_P(\omega)$ and $\varphi_L(\omega)$. This concept is schematically depicted in Fig. 1, showing the different phase contributions for the SFG and DFG pathways along with their corresponding susceptibilities.

Besides the described benefit of gaining direct access to the desired correlated information on depth coordinates and local dielectric environments, there is another important aspect that makes such a phase decomposition often indispensable: by eliminating the extrinsic contributions, the "true," intrinsic response of the molecular systems being probed can be determined with great accuracy. This is particularly relevant for substrates where the extrinsic phase contributions are significant, such as interfaces with a high degree of ordering through large depths, or those at metal surfaces which are strongly absorbing.[13] For example, both of these effects are present in electrochemical systems where the metallic electrodes with applied potentials can lead to substantial extrinsic phase contributions. As a result, the measured (uncorrected) vibrational line-shapes show significant spectral distortions
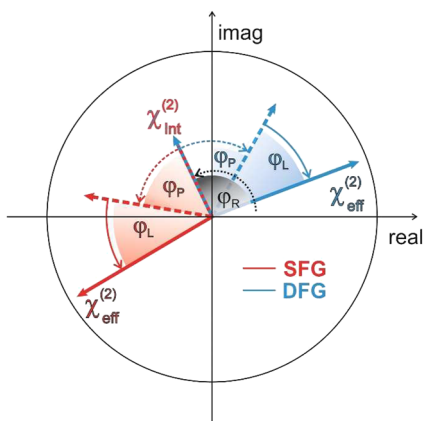
FIG. 1. Schematic depiction of the different phase contributions to the measured susceptibility, $\chi_{eff}^{(2)}$, namely the intrinsic phase, φ_R, the propagation phase, φ_P, and the local field phase, φ_L.

which often largely prohibit a detailed spectral analysis and may easily lead to incorrect interpretations of the obtained results.[14,15] A precise decomposition of the overall measured phase into intrinsic and extrinsic contributions can then efficiently overcome this challenge.

In this contribution, the concept of disentangling the measured phase into its constituents by means of pathway-selective second order measurements is presented theoretically and experimentally. One aspect of this concept has previously been presented for the example of systems containing a propagation phase on non-absorbing substrates (thus possessing no local field phase), where the method was shown to yield high spatial accuracy reaching the sub-nanometre length-scale.[16] Here, the theoretical considerations are generalised and derived from first principles. This includes a quantum-mechanical derivation of the different induced nonlinear polarisations for each pathway, as well as how they are mapped onto to the experimentally measured SFG and DFG signals. Although many theoretical descriptions of nonlinear optics can be found elsewhere in the literature,[9,17–19] the detailed description of both SFG and DFG responses given here extends beyond the general concepts which are commonly presented, particularly through consideration of intrinsic responses arising from a subset of the entire frequency-space, extension of permutation symmetry arguments in the experimentally relevant scenarios of ground state restriction and vibrational resonance, and, importantly, how these intrinsic susceptibilities are related to the measured responses. This sets out the combined SFG/DFG technique on a broad theoretical foundation. The now generalised concept also includes local field phase contributions, which are shown to be equally separable from the intrinsic phase as was the propagation phase. Finally, this concept is experimentally validated by a series of SFG and DFG measurements on selected model samples of self-assembled monolayers (SAMs) formed on metal surfaces, comparing the obtained results with the common theoretical model (three-layer model, 3LM).[18,19]

THEORETICAL CONSIDERATIONS

The technique presented in this work is based on disentangling and extracting components from the phase of the measured second order responses probing different Liouville pathways, specifically the SFG and DFG output fields. As mentioned in the introduction, the response in both cases is described by the effective second order susceptibility, which is markedly different from the intrinsic response that directly arises from the molecular hyperpolarisabilities, as it is also affected by both the driving fields and the emitted field. This distinction between intrinsic and effective responses will be essential for the understanding of the theoretical description of the presented method.

To make meaningful comparisons between the effective SFG and DFG responses, it is important to consider circumstances under which they are equal, and those where they are not. In the following theoretical considerations, the two intrinsic responses will be broken down to their quantum mechanical origins in order to derive the conditions of equality, ultimately showing that this occurs in most cases. Thereafter, the (measured) effective susceptibilities will be compared where they are shown to generally differ for different pathways. These differences originate from the extrinsic phase contributions relating to the interaction of the driving fields with the chromophore in its specific environment [i.e., local field and spatial (depth) origin]. It is thus these deviations between the measured SFG and DFG responses that are exploited in disentangling the intrinsic and extrinsic phase contributions to the effective susceptibility and obtaining the desired information.

As a final note, when contrasting SFG with DFG, there are two distinct and relevant cases that will be addressed. Firstly, SFG and DFG responses can be generated simultaneously within one experimental setting, where both relate to the ***same two input frequencies*** but ***different output frequencies***, as in Eq. (2). Secondly, there are SFG and DFG responses which both involve the ***same three frequencies*** that have just been ***interchanged***, as in Eq. (3), but must arise from two separate experiments since they require different input frequencies. In the following theoretical considerations, both cases will be explored and discussed.

$$\tilde{\chi}^{(2)}(\omega_2 + \omega_1, \omega_2, \omega_1) \quad vs \quad \tilde{\chi}^{(2)}(-\omega_2 + \omega_1, -\omega_2, \omega_1) \qquad (2)$$

$$\tilde{\chi}^{(2)}(\omega_2 + \omega_1, \omega_2, \omega_1) \quad vs \quad \tilde{\chi}^{(2)}(-\omega_2, -\omega_2 - \omega_1, \omega_1) \qquad (3)$$

It is clear that the expressions in Eqs. (2) and (3) only consider half of each conjugate pair of the overall measured SFG and DFG responses, with the other side of each being equivalent, but with negation of the frequency arguments and phase contributions. Whilst the choice of using the specific responses in Eqs. (2) and (3) is due to them both having positive ω_1 (so they can be directly plotted together and have equal resonant phase contributions) and being corresponding terms in the permutation symmetry relations (see later), the choice is otherwise arbitrary and has no impact on the phase disentanglement that is possible through this method. The theoretical considerations presented here can be trivially converted to any other combination of either part of the SFG conjugate pairing with either from the DFG,

purely by flipping the corresponding signs of the frequencies and phases.

A summary of the detailed theoretical descriptions given below is as follows: in the first step, the correlation functions contributing to the intrinsic SFG and DFG responses will be derived quantum mechanically, accounting for ground state restrictions and resonant interactions that are commonplace in vibrational measurements. Secondly, the comparison between the two intrinsic responses will be discussed both from the perspective of permutation symmetry [aligning with Eq. (3)] and for the two responses arising from the same measurement [i.e., Eq. (2)]. Thereafter, the discussion will navigate towards the extrinsic phase contributions, culminating in expressions for the measured SFG and DFG responses being derived and how their comparison can lead to a disentanglement of the intrinsic and extrinsic phase contributions.

Interaction pathways in the second order response

The theory underlying nonlinear optics has been developed and reviewed in great detail, with full descriptions and derivations of the quantum mechanical equations found elsewhere in the literature.[9,17–19] Here, a brief summary of the relevant Liouville pathway considerations is given based on the semi-classical approach for the overall Hamiltonian. Although this can be applied to both comparisons between SFG and DFG [described by Eqs. (2) and (3)], only the simultaneous responses described by Eq. (2) are considered in this part [where the equivalent expressions based on Eq. (3) can be extracted by a simple frequency shift of the two high frequency arguments].

In nonlinear spectroscopies, the generated fields arise through multiple interactions between the incident field(s), which consist of positive and negative frequency components (conjugate pairs), and the molecular dipoles. This describes the interaction Hamiltonian which can be substituted into the Liouville equation to derive different elements of the density matrix after each interaction. The result is that each component of the interaction Hamiltonian, $V = -\mu \cdot E$, (i.e., both positive and negative frequencies) can act on either the bra or ket side of the density matrix, ρ, as shown for the interaction with a single field $E(t)$ resulting in a transition between states "a" and "b" in Eq. (4) (summing over all real states, "p," of the system).

$$\langle b|[V(t), \rho]|a\rangle = -\left(E_n(t) + E_n^*(t)\right) \cdot \sum_p \mu_{bp}\rho_{pa} - \rho_{bp}\mu_{pa} \quad (4)$$

Therefore, for each interaction, there are four unique routes. The positive terms in Eq. (4) involve interaction with the bra side of the density matrix whereas negative terms indicate an interaction with the ket side. Of these, those involving the $E_n(t)$ part of the field correspond to a positive frequency interaction (absorption on the ket side, A_{ket}, and stimulated emission on the bra side, S_{bra}) and those with $E_n^*(t)$ correspond to a negative frequency interaction (stimulated emission on the ket side, S_{ket}, and absorption on the bra side, A_{bra}). It is hence trivial to identify that two interactions with the same field will yield 16 possible pathways, half of which describe second harmonic generation (SHG) and the other half optical rectification (OR).[20–22] A more detailed description of these different pathways, how they relate to the common derivation of the second

order susceptibility, and which are allowed from the ground state can be found in Appendix A.

By extending the concepts above to the case of two interactions with two different fields, one can generate the typical description of the general second order response. The overall second order polarisation, $P^{(2)}(t)$, can be given as in Eq. (5), summing over the different permutations of the incident fields. This contains 16 different $\tilde{\chi}^{(2)}$ components (intrinsic susceptibilities), each with four correlation functions which correspond to unique pathways through Liouville space. As an example, the $\tilde{\chi}^{(2)}(\omega_m + \omega_n, \omega_m, \omega_n)$ component (with all positive frequencies) is contributed to by the correlation functions corresponding to the following four Liouville pathways: $A_{ket}(E_n) \rightarrow A_{ket}(E_m)$, $A_{ket}(E_n) \rightarrow S_{bra}(E_m)$, $S_{bra}(E_n) \rightarrow A_{ket}(E_m)$, and $S_{bra}(E_n) \rightarrow S_{bra}(E_m)$. Overall, therefore, the 16 pathways discussed above for two interactions with the same field are expanded to 64.

$$
\begin{aligned}
P_i^{(2)}(t) = \varepsilon_0 \sum_{m,n}^{1,2} \sum_{j,k}^{x,y,z} &\int_{-\infty}^{\infty} d\omega_m \int_{-\infty}^{\infty} d\omega_n \\
&\tilde{\chi}_{ijk}^{(2)}(\omega_m + \omega_n, \omega_m, \omega_n) : E_j(\omega_m)E_k(\omega_n)e^{-i(\omega_m+\omega_n)t} \\
&+ \tilde{\chi}_{ijk}^{(2)}(\omega_m - \omega_n, \omega_m, -\omega_n) : E_j(\omega_m)E_k^*(\omega_n)e^{-i(\omega_m-\omega_n)t} \\
&+ \tilde{\chi}_{ijk}^{(2)}(-\omega_m + \omega_n, -\omega_m, \omega_n) : E_j^*(\omega_m)E_k(\omega_n)e^{-i(-\omega_m+\omega_n)t} \\
&+ \tilde{\chi}_{ijk}^{(2)}(-\omega_m - \omega_n, -\omega_m, -\omega_n) : E_j^*(\omega_m)E_k^*(\omega_n)e^{-i(-\omega_m-\omega_n)t}
\end{aligned}
$$
$$(5)$$

As discussed in Appendix A for the SHG/OR case, each pathway can be portrayed in a grid format such as that in Table I, with each cell corresponding to a unique correlation function. Note that half correspond to complex conjugates of the other half, and thus will not contain unique information. On assuming an initial ground state population, a reasonable assumption for vibrational spectroscopy as $\omega \gg kT$, the 64 pathways significantly reduce to 22 non-zero terms. These are highlighted in Table I, with four representing SHG (orange), four SFG (red), eight OR (green) and six DFG (blue). The asymmetry between OR and DFG should be noted as arising from two disallowed pathways in the latter [$A_{ket}(E_1) \rightarrow S_{ket}(E_2)$ and its conjugate, $A_{bra}(E_1) \rightarrow S_{bra}(E_2)$] that arise from having two different frequency input fields (where one cannot have stimulated emission of the higher frequency field after absorption of the lower), taking $\omega_2 > \omega_1$ in this case without loss of generality. In the common experimental setup probing vibrational resonances, with infrared and visible input fields [$E(\omega_1)$ and $E(\omega_2)$, respectively], one pair of conjugate pathways for SFG and DFG contains the resonant responses, with the others representing purely non-resonant contributions. This is further highlighted by colouring the resonant pathways in dark red and dark blue, and the non-resonant pathways in pale red and blue in Table I. The allowed SFG and DFG pathways can be represented diagrammatically in the form of Feynman diagrams, ladder diagrams, and Liouville space pathways as shown in Fig. 2, where the same colouring of resonant and non-resonant pathways is included, as well as empha-

TABLE I. Representation of the 64 possible interaction pathways that exist for two interactions with two independent frequency fields present. The "+" and "−" symbols indicate the contribution to the frequency and wave vector of the generated signal field. Highlighted colours are used to indicate the allowed pathways when starting from the ground state, with SHG processes shown in orange, OR in green, SFG in red, and DFG in blue (with the dark and light SFG and DFG pathway colours indicating resonant and non-resonant pathways, respectively).

			Interaction 1							
			$E(\omega_1)$				$E(\omega_2)$			
			Absorption		Stimulated Emission		Absorption		Stimulated Emission	
			Ket	Bra	Ket	Bra	Ket	Bra	Ket	Bra
Interaction 2	$E(\omega_1)$ Absorption	Ket	+1+1	-1+1	-1+1	+1+1	+2+1	-2+1	-2+1	+2+1
		Bra	+1-1	-1-1	-1-1	+1-1	+2-1	-2-1	-2-1	+2-1
	Stimulated Emission	Ket	+1-1	-1-1	-1-1	+1-1	+2-1	-2-1	-2-1	+2-1
		Bra	+1+1	-1+1	-1+1	+1+1	+2+1	-2+1	-2+1	+2+1
	$E(\omega_2)$ Absorption	Ket	+1+2	-1+2	-1+2	+1+2	+2+2	-2+2	-2+2	+2+2
		Bra	+1-2	-1-2	-1-2	+1-2	+2-2	-2-2	-2-2	+2-2
	Stimulated Emission	Ket	+1-2	-1-2	-1-2	+1-2	+2-2	-2-2	-2-2	+2-2
		Bra	+1+2	-1+2	-1+2	+1+2	+2+2	-2+2	-2+2	+2+2

sising the resonant coherence ("*ab*" or "*ba*") in bold and with green highlights.

Correlation functions

As mentioned above, each individual $\tilde{\chi}^{(2)}$ contribution to the overall second order polarisation, corresponding to each combination of positive and negative frequency arguments, contains four correlation functions (pathways) which are summed. However, on restriction to the ground state many of these vanish. For SFG, the four possible combinations of frequency arguments $(\tilde{\chi}^{(2)}(\omega_2 + \omega_1, \omega_2, \omega_1)$, $\tilde{\chi}^{(2)}(-\omega_2 - \omega_1, -\omega_2, -\omega_1)$, $\tilde{\chi}^{(2)}(\omega_1 + \omega_2, \omega_1, \omega_2)$, and $\tilde{\chi}^{(2)}(-\omega_1 - \omega_2, -\omega_1, -\omega_2))$ only end up with a single correlation function each. Similarly, the DFG response is constituted by two elements with a single correlation function and two elements with a pair of correlation functions. Therefore, when considering the contributions to the second order polarisation oscillating at the SFG or DFG frequency [once again only considering the simultaneously generated responses as in Eq. (2), but with those from Eq. (3) being equally obtainable via a simple frequency shift], the overall intrinsic susceptibilities, $\tilde{\chi}^{(2)}_{SFG}$ and $\tilde{\chi}^{(2)}_{DFG}$, can be expressed as a sum over their contributing correlation functions (labelled as C^i). This is expressed in Eqs. (6) and (7), with the explicit expressions for the individual correlation functions given in Eqs. (8a)–(8j) (summing over all the real states of the system with placeholder indices "*p*" and "*q*"). The corresponding correlation
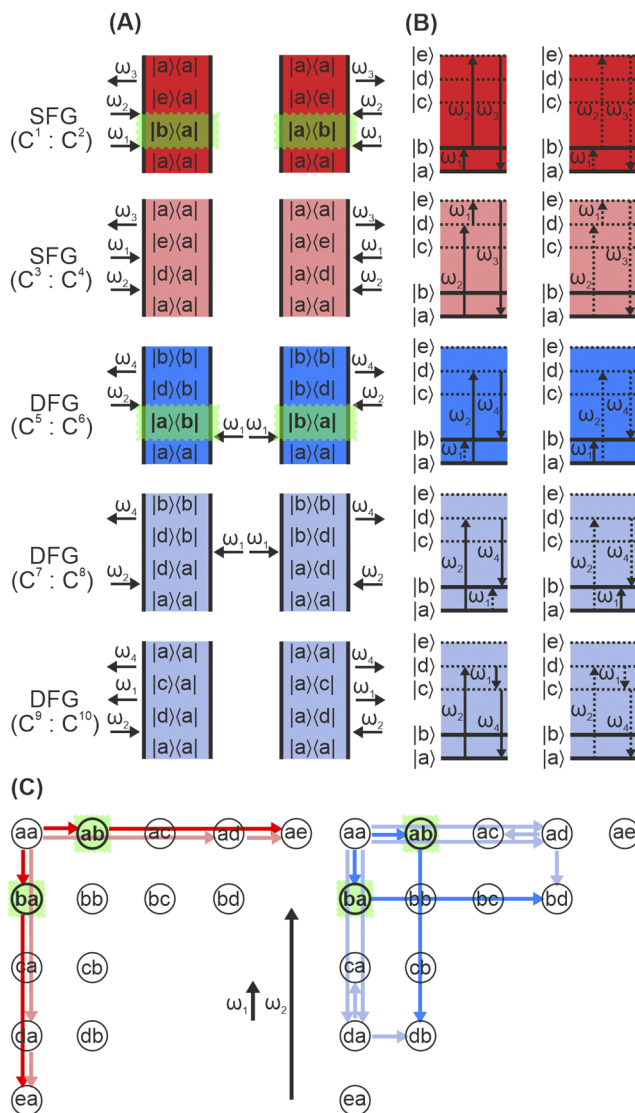

FIG. 2. Representations of the different pathway contributions to the general second order response function when initially in the ground state through two interactions with electric fields oscillating at different frequencies ω_1 and ω_2, showing (a) Feynman diagrams, (b) ladder diagrams, and (c) Liouville space pathways. Taking ω_1 to be resonant, the resonant pathways are indicated with dark shading, and the non-resonant pathways with pale shading, with the real-state coherences ("*ab*" and "*ba*") highlighted in bold and with green highlights in (a) and (c) as the real state energy levels ("*a*" and "*b*") indicated with solid lines and virtual states by dotted lines in (b). The corresponding correlation functions, C^1–C^{10}, for the individual pathways explicitly shown in (a) and (b) are indicated on the left.

function from Eq. (8) is also indicated for each pathway shown in Fig. 2.

$$\tilde{\chi}^{(2)}_{SFG} = C^1 + C^2 + C^3 + C^4 \quad (6)$$

$$\tilde{\chi}^{(2)}_{DFG} = C^5 + C^6 + C^7 + C^8 + C^9 + C^{10} \tag{7}$$

$$C^1_{ijk}(\omega_2 + \omega_1, \omega_2, \omega_1)$$
$$= \frac{N}{2\varepsilon_0\hbar^2}\sum_{p,q} \frac{\mu^i_{aq}\mu^j_{qp}\mu^k_{pa}}{(\omega_1 - \omega_{pa} + i\Gamma_{pa})(\omega_2 + \omega_1 - \omega_{qa} + i\Gamma_{qa})} \tag{8a}$$

$$C^2_{ijk}(-\omega_2 - \omega_1, -\omega_2, -\omega_1)$$
$$= \frac{N}{2\varepsilon_0\hbar^2}\sum_{p,q} \frac{\mu^i_{qa}\mu^j_{pq}\mu^k_{ap}}{(-\omega_1 - \omega_{ap} + i\Gamma_{ap})(-\omega_2 - \omega_1 - \omega_{aq} + i\Gamma_{aq})} \tag{8b}$$

$$C^3_{ijk}(\omega_1 + \omega_2, \omega_1, \omega_2)$$
$$= \frac{N}{2\varepsilon_0\hbar^2}\sum_{p,q} \frac{\mu^i_{aq}\mu^j_{qp}\mu^k_{pa}}{(\omega_2 - \omega_{pa} + i\Gamma_{pa})(\omega_1 + \omega_2 - \omega_{qa} + i\Gamma_{qa})} \tag{8c}$$

$$C^4_{ijk}(-\omega_1 - \omega_2, -\omega_1, -\omega_2)$$
$$= \frac{N}{2\varepsilon_0\hbar^2}\sum_{p,q} \frac{\mu^i_{qa}\mu^j_{pq}\mu^k_{ap}}{(-\omega_2 - \omega_{ap} + i\Gamma_{ap})(-\omega_1 - \omega_2 - \omega_{aq} + i\Gamma_{aq})} \tag{8d}$$

$$C^5_{ijk}(\omega_2 - \omega_1, \omega_2, -\omega_1)$$
$$= \frac{-N}{2\varepsilon_0\hbar^2}\sum_{p,q} \frac{\mu^i_{pq}\mu^j_{qa}\mu^k_{ap}}{(-\omega_1 - \omega_{ap} + i\Gamma_{ap})(\omega_2 - \omega_1 - \omega_{qp} + i\Gamma_{qp})} \tag{8e}$$

$$C^6_{ijk}(-\omega_2 + \omega_1, -\omega_2, \omega_1)$$
$$= \frac{-N}{2\varepsilon_0\hbar^2}\sum_{p,q} \frac{\mu^i_{qp}\mu^j_{aq}\mu^k_{pa}}{(\omega_1 - \omega_{pa} + i\Gamma_{pa})(-\omega_2 + \omega_1 - \omega_{pq} + i\Gamma_{pq})} \tag{8f}$$

$$C^7_{ijk}(-\omega_1 + \omega_2, -\omega_1, \omega_2)$$
$$= \frac{-N}{2\varepsilon_0\hbar^2}\sum_{p,q} \frac{\mu^i_{qp}\mu^j_{aq}\mu^k_{pa}}{(\omega_2 - \omega_{pa} + i\Gamma_{pa})(-\omega_1 + \omega_2 - \omega_{pq} + i\Gamma_{pq})} \tag{8g}$$

$$C^8_{ijk}(\omega_1 - \omega_2, \omega_1, -\omega_2)$$
$$= \frac{-N}{2\varepsilon_0\hbar^2}\sum_{p,q} \frac{\mu^i_{pq}\mu^j_{qa}\mu^k_{ap}}{(-\omega_2 - \omega_{ap} + i\Gamma_{ap})(\omega_1 - \omega_2 - \omega_{qp} + i\Gamma_{qp})} \tag{8h}$$

$$C^9_{ijk}(-\omega_1 + \omega_2, -\omega_1, \omega_2)$$
$$= \frac{N}{2\varepsilon_0\hbar^2}\sum_{p,q} \frac{\mu^i_{aq}\mu^j_{qp}\mu^k_{pa}}{(\omega_2 - \omega_{pa} + i\Gamma_{pa})(-\omega_1 + \omega_2 - \omega_{qa} + i\Gamma_{qa})} \tag{8i}$$

$$C^{10}_{ijk}(\omega_1 - \omega_2, \omega_1, -\omega_2)$$
$$= \frac{N}{2\varepsilon_0\hbar^2}\sum_{p,q} \frac{\mu^i_{qa}\mu^j_{pq}\mu^k_{ap}}{(-\omega_2 - \omega_{ap} + i\Gamma_{ap})(\omega_1 - \omega_2 - \omega_{aq} + i\Gamma_{aq})} \tag{8j}$$

With this quantum mechanical description of the overall second order response in hand, the intrinsic responses of SFG and DFG can be directly compared.

Permutation symmetry with restriction to the ground state

Closer inspection of Eq. (3) shows that the SFG and DFG responses are closely related to permutations of the three frequency arguments. For a full comparison between the two pathways, it is therefore important to discuss permutation symmetry of the intrinsic susceptibilities.

As shown previously in the literature,[17] the $\chi^{(2)}$ response has intrinsic permutation symmetry associated with swapping the two input frequency arguments along with their corresponding indices, as shown in Eq. (9). This symmetry is always valid.

$$\tilde{\chi}^{(2)}_{ijk}(\omega_2 + \omega_1, \omega_2, \omega_1) = \tilde{\chi}^{(2)}_{ikj}(\omega_2 + \omega_1, \omega_1, \omega_2) \tag{9}$$

Furthermore, in the case of fully off-resonant interactions, there is full permutation symmetry where *any* pair of frequency arguments (including the output field) can be interchanged along with their corresponding indices without changing $\chi^{(2)}$ as long as the relationship between input and output frequencies is preserved [as in Eq. (10)].

$$\tilde{\chi}^{(2)}_{ijk}(\omega_2 + \omega_1, \omega_2, \omega_1) = \tilde{\chi}^{(2)}_{jik}(-\omega_2, -\omega_2 - \omega_1, \omega_1)$$
$$= \tilde{\chi}^{(2)}_{kji}(-\omega_1, \omega_2, -\omega_2 - \omega_1)$$
$$= \tilde{\chi}^{(2)}_{ikj}(\omega_1 + \omega_2, \omega_1, \omega_2) \tag{10}$$

A proof of this symmetry relation can be found elsewhere,[17] however two important factors which relate to common experimental settings are often not considered. Firstly, when one of the input frequencies is probing resonances, as typically is the case in SFG, it is not clear to what extent any permutation symmetry survives (other than the intrinsic permutation symmetry). Furthermore, when probing vibrational transitions, the initial state of the system can be assumed to be the ground state, which hence restricts the contributions to the susceptibility, as discussed above. It is also not clear if this restriction leads to any further reduction in symmetry. In the following, it is shown that permutation symmetry is still applicable as long as the two interchanged frequency arguments (and their indices) are non-resonant, irrespective of the resonant status of the third or the initial state of the system.

On restriction to the ground state and only considering the allowed pathways with positive ω_1, i.e., half of each conjugate pair, the intrinsic SFG susceptibility can be expressed as in Eq. (11) [with terms (11a) and (11b) corresponding to the C^1 and C^3 correlation functions].

$$\tilde{\chi}^{(2)}_{ijk}(\omega_2 + \omega_1, \omega_2, \omega_1)$$
$$= \frac{N}{2\varepsilon_0\hbar^2}\sum_{qr} \frac{\mu^i_{gr}\mu^j_{rq}\mu^k_{qg}}{(\omega_1 - \omega_{qg} + i\Gamma_{qg})(\omega_2 + \omega_1 - \omega_{rg} + i\Gamma_{rg})} \tag{11a}$$

$$+ \frac{\mu^i_{gr}\mu^j_{qg}\mu^k_{rq}}{(\omega_2 - \omega_{qg} + i\Gamma_{qg})(\omega_2 + \omega_1 - \omega_{rg} + i\Gamma_{rg})} \tag{11b}$$

Similarly, for DFG, the intrinsic susceptibility [with deliberately swapped indices "i" and "j" and different upconversion frequency compared to the SFG in Eq. (11)] can be written as the sum over the

three allowed correlation functions with positive ω_1 (i.e., C^6, C^8, and C^{10}), as in Eq. (12).

$$\tilde{\chi}^{(2)}_{jik}(-\omega_2, -\omega_2 - \omega_1, \omega_1)$$

$$= \frac{N}{2\varepsilon_0 \hbar^2} \sum_{qr} - \frac{\mu^i_{gr}\mu^j_{rq}\mu^k_{qg}}{(\omega_1 - \omega_{qg} + i\Gamma_{qg})(-\omega_2 - \omega_{qr} + i\Gamma_{qr})} \quad (12a)$$

$$- \frac{\mu^i_{gq}\mu^j_{qr}\mu^k_{rg}}{(-\omega_2 - \omega_1 - \omega_{gq} + i\Gamma_{gq})(-\omega_2 - \omega_{rq} + i\Gamma_{rq})} \quad (12b)$$

$$+ \frac{\mu^i_{gq}\mu^j_{rg}\mu^k_{qr}}{(-\omega_2 - \omega_1 - \omega_{gq} + i\Gamma_{gq})(-\omega_2 - \omega_{gr} + i\Gamma_{gr})} \quad (12c)$$

By manipulating the signs of the individual terms, Eq. (12) can be rewritten as in Eq. (13).

$$\tilde{\chi}^{(2)}_{jik}(-\omega_2, -\omega_2 - \omega_1, \omega_1)$$

$$= \frac{N}{2\varepsilon_0 \hbar^2} \sum_{qr} \frac{\mu^i_{gr}\mu^j_{rq}\mu^k_{qg}}{(\omega_1 - \omega_{qg} + i\Gamma_{qg})(\omega_2 - \omega_{rq} - i\Gamma_{rq})} \quad (13a)$$

$$- \frac{\mu^i_{gq}\mu^j_{qr}\mu^k_{rg}}{(\omega_2 + \omega_1 - \omega_{qg} - i\Gamma_{qg})(\omega_2 - \omega_{qr} - i\Gamma_{qr})} \quad (13b)$$

$$+ \frac{\mu^i_{gq}\mu^j_{rg}\mu^k_{qr}}{(\omega_2 + \omega_1 - \omega_{qg} - i\Gamma_{qg})(\omega_2 - \omega_{rg} - i\Gamma_{rg})} \quad (13c)$$

Then, swapping the dummy indices, "q" and "r," in the terms (13b) and (13c), followed by factorisation of the first two terms results in Eq. (14).

$$\tilde{\chi}^{(2)}_{jik}(-\omega_2, -\omega_2 - \omega_1, \omega_1)$$

$$= \frac{N}{2\varepsilon_0 \hbar^2} \sum_{qr} \frac{\mu^i_{gr}\mu^j_{rq}\mu^k_{qg}}{\omega_2 - \omega_{rq} - i\Gamma_{rq}}$$

$$\times \left\{ \frac{1}{\omega_1 - \omega_{qg} + i\Gamma_{qg}} - \frac{1}{\omega_2 + \omega_1 - \omega_{rg} - i\Gamma_{rg}} \right\} \quad (14a)$$

$$+ \frac{\mu^i_{gr}\mu^j_{qg}\mu^k_{rq}}{(\omega_2 + \omega_1 - \omega_{rg} - i\Gamma_{rg})(\omega_2 - \omega_{qg} - i\Gamma_{qg})} \quad (14b)$$

The term in curly brackets in Eq. (14) [term (14a)] can then be trivially manipulated to yield term (15a) in Eq. (15).

$$\tilde{\chi}^{(2)}_{jik}(-\omega_2, -\omega_2 - \omega_1, \omega_1)$$

$$= \frac{N}{2\varepsilon_0 \hbar^2} \sum_{qr} \frac{\mu^i_{gr}\mu^j_{rq}\mu^k_{qg}}{\omega_2 - \omega_{rq} - i\Gamma_{rq}}$$

$$\times \left\{ \frac{\omega_2 - \omega_{rq} - i(\Gamma_{rg} + \Gamma_{qg})}{(\omega_1 - \omega_{qg} + i\Gamma_{qg})(\omega_2 + \omega_1 - \omega_{rg} - i\Gamma_{rg})} \right\} \quad (15a)$$

$$+ \frac{\mu^i_{gr}\mu^j_{qg}\mu^k_{rq}}{(\omega_2 + \omega_1 - \omega_{rg} - i\Gamma_{rg})(\omega_2 - \omega_{qg} - i\Gamma_{qg})} \quad (15b)$$

Clearly, the expressions in Eq. (15) are different from the corresponding SFG terms [Eq. (11)]. However, in the case that the two high frequency interactions are far from resonance, Eqs. (11) and (15) can be simplified into Eqs. (16) and (17), respectively.

$$\tilde{\chi}^{(2)}_{ijk}(\omega_2 + \omega_1, \omega_2, \omega_1)$$

$$= \frac{N}{2\varepsilon_0 \hbar^2} \sum_{qr} \frac{1}{(\omega_2 + \omega_1 - \omega_{rg})} \left(\frac{\mu^i_{gr}\mu^j_{rq}\mu^k_{qg}}{\omega_1 - \omega_{qg} + i\Gamma_{qg}} + \frac{\mu^i_{gr}\mu^j_{qg}\mu^k_{rq}}{\omega_2 - \omega_{qg}} \right)$$

$$= \sum_{qr} G_r(\omega_2, \omega_1) \left(R_{rq}(\omega_1) e^{i\phi_q(\omega_1)} + NR_{rq}(\omega_2) \right) \quad (16)$$

In both equations the response has been factorised by the frequency-dependent real pre-factor, G, with both the resonant and non-resonant terms being written in polar coordinates with amplitudes of R and NR, respectively, and the resonant phase, ϕ. Here it is important to note that although R is labelled as resonant and NR non-resonant, both contributions are expressed as the sum over all states and thus must both contain off-resonant terms. The only difference is that only the former **contains** the term contributing the resonant line-shape(s) whereas the latter is purely non-resonant.

$$\tilde{\chi}^{(2)}_{jik}(-\omega_2, -\omega_2 - \omega_1, \omega_1)$$

$$= \frac{N}{2\varepsilon_0 \hbar^2} \sum_{qr} \frac{1}{(\omega_2 + \omega_1 - \omega_{rg})}$$

$$\times \left(\frac{\mu^i_{gr}\mu^j_{rq}\mu^k_{qg}}{\omega_1 - \omega_{qg} + i\Gamma_{qg}} + \frac{\mu^i_{gr}\mu^j_{qg}\mu^k_{rq}}{\omega_2 - \omega_{qg}} \right)$$

$$= \sum_{qr} G_r(\omega_2, \omega_1) \left(R_{rq}(\omega_1) e^{i\phi_q(\omega_1)} + NR_{rq}(\omega_2) \right) \quad (17)$$

Comparing the responses in Eqs. (16) and (17) shows that they are indeed identical. (NB: Since this is true for the summation of half of each conjugate pair, it must therefore also hold for the other half, and thus also for the total response.) From this, it is clear that swapping the two off-resonant frequencies leads to the same result, showing that a remnant of full permutation symmetry survives (hereafter described as partial permutation symmetry). Based on this finding it can be followed that the intrinsic SFG and DFG responses containing the same two off-resonant frequencies [Eq. (3) discussed above] are precisely equal as long as swapping the indices "i" and "j" has no impact on the susceptibility. This restriction is not problematic when the tensor components being probed can be expressed as χ_{aab}. This is always the case for the SSP polarisation combination which is common in experimental applications of SFG and DFG. Even for PPP, which is also commonly applied, the four contributions for rotationally isotropic media fulfil this criterion to a good approximation as the signals are dominated by the ZZZ and XXZ components (with the XZX and ZXX highly cancelling, assuming a co-propagating beam geometry).[23] With regards to other polarisation combinations which are sometimes used, such as SPS or PSS, or even PSP and SPP for chiral systems, they clearly do not satisfy the partial permutation symmetry and, therefore, any comparison between SFG and DFG should consider the relative similarity of the product of the two transition dipole

moments ($\mu_{gr}^i \mu_{rq}^j$) when using opposite polarisations. It should also be noted that the same partial permutation symmetry, with one input being resonant, also holds when the ground state restriction is lifted, as shown in Appendix B.

Such SFG and DFG experiments can be carried out, but this requires two separate measurements [as mentioned earlier, see Eq. (3)]. More convenient are often experiments where SFG and DFG are measured simultaneously [see Eq. (2)]. For the correct comparison of the two responses in this case, however, Eq. (17) must be modified as this goes beyond pure permutation of the three frequency arguments (it additionally involves frequency shifting). The DFG response is then described by Eq. (18).

$$
\begin{aligned}
\tilde{\chi}_{jik}^{(2)}(-\omega_2 + \omega_1, -\omega_2, \omega_1) &= \frac{N}{2\varepsilon_0 \hbar^2} \sum_{qr} \frac{1}{(\omega_2 - \omega_{rg})} \left(\frac{\mu_{gr}^i \mu_{rq}^j \mu_{qg}^k}{\omega_1 - \omega_{qg} + i\Gamma_{qg}} + \frac{\mu_{gr}^i \mu_{qg}^j \mu_{rq}^k}{\omega_2 - \omega_1 - \omega_{qg}} \right) \\
&= \sum_{qr} G_r'(\omega_2, \omega_1) \left(R_{rq}(\omega_1) e^{i\phi_q(\omega_1)} + NR_{rq}'(\omega_2) \right) \\
&= \sum_{qr} \left(1 + \frac{\omega_1}{\omega_2 - \omega_{rg}} \right) G_r(\omega_2, \omega_1) \left(R_{rq}(\omega_1) e^{i\phi_q(\omega_1)} + \left(1 + \frac{\omega_1}{\omega_2 - \omega_1 - \omega_{qg}} \right) NR_{rq}(\omega_2) \right)
\end{aligned}
\tag{18}
$$

By comparing Eq. (18) with Eq. (17) it is clear that the only difference in the two DFG responses arises from the real pre-factors, and a real amplitude scaling of the (purely) non-resonant contribution. It is important to notice that the resonant response is completely unaltered, both in line-shape and phase. Furthermore, as the pre-factors are non-resonant, their variations are dominated by the experimental parameters and not the sample properties and thus should be removed through referencing, and any dispersion in the purely non-resonant term should be vanishingly small considering it is typically dominated by high-lying electronic states.[24] Therefore, this shows that, just like the permutation-type DFG response [Eq. (3)], the simultaneously obtained DFG response [Eq. (2)] has an identical resonant term to the SFG. Hence, it matters not which pair of SFG and DFG responses are used for comparison in an experiment, the respective intrinsic susceptibilities should be equal. Nevertheless, as the permutation-type DFG response [Eq. (3)] is exactly equal to the SFG response regardless of referencing, this comparison will be used in the experimental part of this publication for greater accuracy and generality.

The measured effective susceptibility

The theoretical considerations thus far set out the intrinsic second order response for SFG and DFG, concluding that they must be equal under the conditions described above. However, in an experiment one does not simply measure the intrinsic responses driven by the input fields, but instead, obtains nonlinear signals reflecting the effective susceptibility. As described earlier, alongside the intrinsic susceptibility, the important modulations of the driving and generated fields as they are delivered to the local chromophore and detector are also encoded in the measured response. These modulations include interactions with surrounding material, typically being described by the nonlinear Fresnel factors, as well as a propagation term arising from the sum of all individual optical pathways to/from individual chromophores. Both of these effects can add significant phase and amplitude contributions which modify the measured (effective) susceptibilities for SFG and DFG, resulting in deviations between the two.

In order to derive the effective susceptibility, the complex nonlinear Fresnel factors, $L(\omega, z)$, are introduced, where the z-dependence is included to account for any variation of the dielectric function with depth. Additionally, the spatial (depth) coordinates of the intrinsic susceptibilities are included, resulting in magnitude changes that manifest as a depth dependency to $|\chi|$ and phase changes that are explicitly included in the propagation phase term, φ_P. With these inclusions, the measured susceptibility, $\chi^{(2)'}(\omega_c, \omega_b, \omega_a)$, can be written as in Eq. (19), where the integration is performed over infinite depth to account for any and all contributions from chromophores. Here, for greater generality, the frequency arguments ω_b and ω_a are used to represent any of the possible input frequencies (i.e., $\pm\omega_1$ or $\pm\omega_2$) with the output frequency, ω_c, defined by $\omega_c = \omega_b + \omega_a$. The Fresnel factors are expressed in polar coordinates, allowing the phase to be explicitly included.

$$
\begin{aligned}
&\chi_{ijk}^{(2)'}(\omega_c, \omega_b, \omega_a) \\
&= \int dz \left| L_{ii}(\omega_c, z) L_{jj}(\omega_b, z) L_{kk}(\omega_a, z) \tilde{\chi}_{ijk}^{(2)}(\omega_c, \omega_b, \omega_a, z) \right| \\
&\quad \times e^{i(\varphi_R(\omega_c, \omega_b, \omega_a, z) + \varphi_P(\omega_c, \omega_b, \omega_a, z) + \varphi_L(\omega_c, \omega_b, \omega_a, z))}
\end{aligned}
\tag{19}
$$

The propagation phase contribution in Eq. (19) can be further expressed as, $\varphi_P(\omega_c, \omega_b, \omega_a, z) = \Delta k_z z$ with the wave vector mismatch Δk_z and the spatial (depth) coordinate of the chromophore z. Furthermore, the overall Fresnel factor phase can be broken down into its three (single frequency) components, $\varphi_L(\omega_c, \omega_b, \omega_a, z) = \varphi_L(\omega_c, z) + \varphi_L(\omega_b, z) + \varphi_L(\omega_a, z)$.

If one now compares the measurement of both SFG and DFG Liouville pathways with a positive resonant frequency, $\omega_a = +\omega_1$, i.e. $\chi_{ijk}^{(2)'}(\omega_2 + \omega_1, \omega_2, \omega_1)$ and $\chi_{ijk}^{(2)'}(-\omega_2, -\omega_2 - \omega_1, \omega_1)$, then the intrinsic phase is the same in both responses (as shown earlier). By

contrast, when in a reflection geometry, the propagation phase will have opposite signs, as shown in Eqs. (20) and (21).

$$\varphi_P^{SFG} = (|k_z(\omega_1)| + |k_z(\omega_2)| + |k_z(\omega_2 + \omega_1)|)z > 0 \tag{20}$$

$$\varphi_P^{DFG} = (|k_z(\omega_1)| - |k_z(\omega_2 + \omega_1)| - |k_z(\omega_2)|)z < 0 \tag{21}$$

Similarly, a sign flip in the argument for any of the Fresnel factors is equivalent to taking the complex conjugate since they are related to the linear interaction with the corresponding field,[1] which

thus flips the sign of the corresponding phase contribution, as in Eq. (22).

$$L_{nn}(-\omega) = L_{nn}(\omega)^* = \left(|L_{nn}(\omega)|e^{i\varphi_L(\omega)}\right)^* = |L_{nn}(\omega)|e^{-i\varphi_L(\omega)} \tag{22}$$

Therefore, in this case, the expressions for the measured susceptibility in SFG and DFG are given by Eqs. (23) and (24), respectively, also applying the partial permutation symmetry of the intrinsic response for DFG (as shown earlier).

$$\chi_{ijk}^{(2)\prime}(\omega_2 + \omega_1, \omega_2, \omega_1) = \int dz \left| L_{ii}(\omega_2 + \omega_1, z) L_{jj}(\omega_2, z) L_{kk}(\omega_1, z) \tilde{\chi}_{ijk}^{(2)}(\omega_2 + \omega_1, \omega_2, \omega_1, z) \right|$$
$$\times e^{i\left(\varphi_R(\omega_2 + \omega_1, \omega_2, \omega_1, z) + |\varphi_P^{SFG}| + \varphi_L(\omega_2 + \omega_1, z) + \varphi_L(\omega_2, z) + \varphi_L(\omega_1, z)\right)} \tag{23}$$

$$\chi_{ijk}^{(2)\prime}(-\omega_2, -\omega_2 - \omega_1, \omega_1) = \int dz \left| L_{ii}(\omega_2, z) L_{jj}(\omega_2 + \omega_1, z) L_{kk}(\omega_1, z) \tilde{\chi}_{jik}^{(2)}(\omega_2 + \omega_1, \omega_2, \omega_1, z) \right|$$
$$\times e^{i\left(\varphi_R(\omega_2 + \omega_1, \omega_2, \omega_1, z) - |\varphi_P^{DFG}| - \varphi_L(\omega_2 + \omega_1, z) - \varphi_L(\omega_2, z) + \varphi_L(\omega_1, z)\right)} \tag{24}$$

Comparing Eqs. (23) and (24) shows that SFG and DFG clearly deviate and that this difference entirely arises from the sign flip in certain phase contributions (for the common cases where $i = j$, as discussed previously). This property makes the different phase contributions distinguishable and thus accessible via the measurement of both responses. However, for an arbitrarily complex system and without simplifying assumptions it would be challenging to unambiguously extract the different phase contributions. Nevertheless, many systems of interest typically allow significant simplifications. These can be generally described by two cases, as discussed below.

The first case (case 1) considers completely transparent media in the high frequency region (corresponding to $\omega_2 + \omega_1$ and ω_2), where the two high frequency Fresnel factors become real and thus possess no phase contributions. On the assumption of little variation of the Fresnel factors through the depth (which is reasonable for many systems, e.g., liquid interfaces where the refractive indices typically change over the order of a nanometre[25]), Eqs. (23) and (24) can thus be simplified to Eqs. (25) and (26).

$$\chi_{ijk}^{(2)\prime}(\omega_2 + \omega_1, \omega_2, \omega_1) = \int dz \left| L_{ii}(\omega_2 + \omega_1) L_{jj}(\omega_2) L_{kk}(\omega_1) \right.$$
$$\times \tilde{\chi}_{ijk}^{(2)}(\omega_2 + \omega_1, \omega_2, \omega_1, z) \Big|$$
$$\times e^{i\left(\varphi_R(\omega_2 + \omega_1, \omega_2, \omega_1, z) + \varphi_L(\omega_1) + |\varphi_P^{SFG}|\right)} \tag{25}$$

$$\chi_{ijk}^{(2)\prime}(-\omega_2, -\omega_2 - \omega_1, \omega_1) = \int dz \left| L_{ii}(\omega_2) L_{jj}(\omega_2 + \omega_1) L_{kk}(\omega_1) \right.$$
$$\times \tilde{\chi}_{jik}^{(2)}(\omega_2 + \omega_1, \omega_2, \omega_1, z) \Big|$$
$$\times e^{i\left(\varphi_R(\omega_2 + \omega_1, \omega_2, \omega_1, z) + \varphi_L(\omega_1) - |\varphi_P^{DFG}|\right)} \tag{26}$$

This shows that the only difference between the SFG and DFG responses now originates from the propagation phases which have opposite signs and different amplitudes (different $|\Delta k_z|$). It is worth noting that the Fresnel factor for the IR frequency remains complex in these considerations, but also yields equal contributions to both the SFG and DFG responses. They therefore do not contribute to the difference between the two responses. As shown in Eqs. (20) and (21), there is a linear relationship between the propagation phase terms and z, with the scaling factors, Δk_z, being easily calculable. This means that the isolated depth coordinate, z', of the chromophores becomes accessible. To reach a full analytical solution, the integration must be performed, requiring the application of a functional form for the z-dependence of $\chi^{(2)}$. There are several ways to approach this, with two important cases being discussed here.

In many sample systems the chromophores are located at well-defined depth coordinates, such that their distribution can be taken to be a delta-function (e.g., monolayer systems). In these cases, the integral can be omitted and the phase difference directly yields the depth coordinate, as shown previously with down to sub-nanometre resolution.[16] Alternatively, the transition from an interface to the bulk can give rise to decaying $\chi^{(2)}$ contributions (e.g., liquid interfaces), which may be modelled by an exponential decay function with a defining decay constant. In this case, the decay constant can be extracted, as shown previously.[16]

A second set of simplifications (case 2) to the general expressions shown in Eqs. (23) and (24) can be made for situations where molecular species are highly localised at the interface to absorbing media. Here, although the Fresnel factors are now generally complex, the propagation effects can be assumed to be negligible. This

renders Eqs. (23) and (24) to be as in Eqs. (27) and (28).

$$
\chi_{ijk}^{(2)\prime}(\omega_2 + \omega_1, \omega_2, \omega_1)
$$
$$
= \left| L_{ii}(\omega_2 + \omega_1) L_{jj}(\omega_2) L_{kk}(\omega_1) \tilde{\chi}_{ijk}^{(2)}(\omega_2 + \omega_1, \omega_2, \omega_1) \right|
$$
$$
\times e^{i(\varphi_R(\omega_2 + \omega_1, \omega_2, \omega_1) + \varphi_L(\omega_1) + \varphi_L(\omega_2 + \omega_1) + \varphi_L(\omega_2))}
\tag{27}
$$

$$
\chi_{ijk}^{(2)\prime}(-\omega_2, -\omega_2 - \omega_1, \omega_1)
$$
$$
= \left| L_{ii}(\omega_2) L_{jj}(\omega_2 + \omega_1) L_{kk}(\omega_1) \tilde{\chi}_{jik}^{(2)}(\omega_2 + \omega_1, \omega_2, \omega_1) \right|
$$
$$
\times e^{i(\varphi_R(\omega_2 + \omega_1, \omega_2, \omega_1) + \varphi_L(\omega_1) - \varphi_L(\omega_2 + \omega_1) - \varphi_L(\omega_2))}
\tag{28}
$$

Now, the difference between the two responses is entirely given by the sign flip for the two phase contributions from the high frequency Fresnel factors. Hence, these can be explicitly determined. Note that here the partial permutation symmetry of the intrinsic responses is used, despite this case being for absorbing media (in the visible) where this symmetry does not hold. However, it is important to emphasise that the intrinsic responses to which this symmetry is applied is the response of the molecular chromophore (not absorbing in the visible) and not that of its (absorbing) surroundings. If the absorbing medium itself generates a signal, it adds a second contribution to the overall susceptibility which needs need to be treated separately.

As demonstrated above, measuring both the SFG and DFG responses clearly separates the overall measured phase into two terms, one constituting the intrinsic phase with the phase of the IR Fresnel factor, and the other combining the propagation phase with the phases of the high frequency Fresnel factors. This, separation allows for extraction of the desired spectroscopic information under the described circumstances and/or for the removal of these extrinsic phase effects in order to obtain the intrinsic vibrational response of the system under investigation.

EXPERIMENTAL DEMONSTRATION

The theory outlined above has previously been shown to successfully separate the intrinsic phase from the propagation phase (i.e., case 1 of the simplifications to the general expressions discussed above), resulting in depth-profiling of the resonant chromophores.[16] The work shown here demonstrates that phase disentanglement is possible through this methodology for the other simplified case, i.e., case 2 where the samples contain strongly absorbing substrates but contribute no propagation phase. For this, model systems of 1-octadecanethiol (ODT) self-assembled monolayers (SAMs) on metallic substrates (silver, platinum, copper, and gold) were probed. Due to the complex refractive indices of the metal substrates which persist across the entire electromagnetic spectrum significant phase deviations can be expected for these samples. By contrast, a sample of octadecyltrichlorosilane (OTS) monolayers on fused silica (FS) possesses no phase contributions from the high frequency local fields and thus served as a comparative reference sample. A schematic for these sample systems is shown in Fig. 3.

Both SFG and DFG were measured in the PPP polarisation combination and performed with phase resolution so that each effective susceptibility is only mapped in half of frequency space
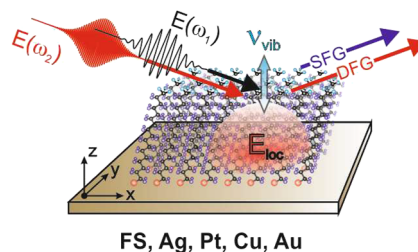

FIG. 3. Schematic showing the model system used to demonstrate the disentanglement of the resonant and local field phase contributions.

corresponding to positive ω_1. For maximum accuracy all experiments are performed using the frequency permutation case [Eq. (3)]. For both pathways, the resulting spectra from the well-packed and highly ordered SAMs are expected to only show the vibrational resonances of the terminal methyl groups[8] and thus have no signal from the depth. Such spectra typically consist of three bands, the first at ~2880 cm^{-1} corresponding to the symmetric CH$_3$ stretch, a subsequent band at ~2940 cm^{-1} due to a Fermi resonance of the symmetric CH$_3$ stretch with a bending mode overtone, and finally the asymmetric CH$_3$ stretch (composed of both the in-plane and out-of-plane modes) at ~2960 cm^{-1}.[8] As shown in the theory section, these systems should possess the same intrinsic phases in their vibrationally resonant response, and thus any deviations in the line-shapes between SFG and DFG can only originate from the phases of the local fields.

Figure 4 shows the corresponding experimentally determined SFG and DFG spectra, split into their real and imaginary parts (dispersive and absorptive line-shapes, respectively) obtained for ODT monolayers atop the four metals substrates (Ag, Pt, Cu, Au). Also included are the reference spectra of the OTS monolayer on FS. As
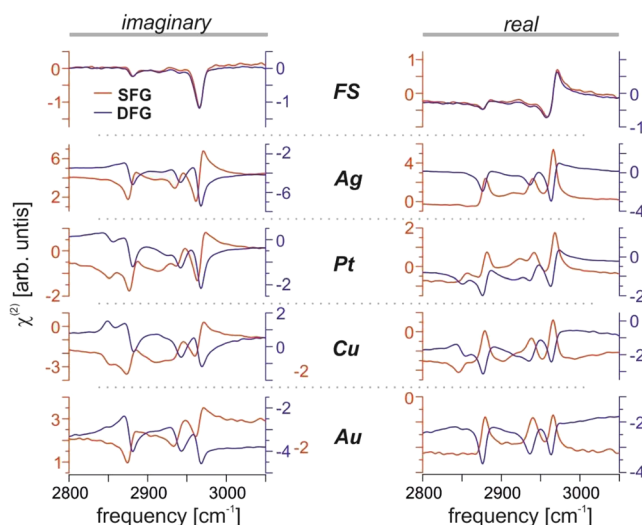

FIG. 4. Phase-resolved SFG and DFG spectra, split into their real and imaginary parts, for four samples of an ODT SAM formed on a metal (Ag, Pt, Cu, and Au) in addition to OTS formed on fused silica (FS).

expected, the SFG and DFG spectra highly overlap for the FS sample since the nonlinear Fresnel factors are entirely real in this case. In contrast, substantial deviations are observed for all four metal samples. Not only do real and imaginary parts of the vibrational line-shapes seem intermixed, but these mixtures also vary for the different samples. This clearly demonstrates the strong effects local fields have on the measured line-shapes.

In order to extract the local field phase values for each sample, a detailed analysis of the different contributions to the measured susceptibilities is required. In the PPP polarisation combination for metallic substrates, the measured susceptibility is strongly dominated by the $\chi_{zzz}^{(2)'}$ component (thus taking $i = j = k = z$)[1] and features the resonant response from the monolayer located at $z = 0$. Besides the resonant response, the strongly absorbing metal substrates also generate a strong (vibrationally) non-resonant contribution due to the substantial polarizability of the delocalised electrons in the metal.[8,15] Hence, the presence of this second contribution somewhat alters the expressions for the measured susceptibility outlined in the theory section. For the required modification of Eqs. (27) and (28) it needs to be considered that, in contrast to the resonant term, the non-resonant contributions from the metals will not follow the partial permutation symmetry of the high frequencies as they are no longer far from resonance in the visible (surface plasmon resonances and inter-band transitions, for example[26]). Another particularity of such nonlinear measurements on metal surfaces which needs to be considered are field enhancement effects[27] that can lead to different scaling of SFG and DFG responses. Overall, the susceptibilities can then be written as in Eqs. (29) and (30)

$$\chi_{PPP}^{(2)'}(\omega_2 + \omega_1, \omega_2, \omega_1)$$
$$= \left\{ \left| \tilde{\chi}_{zzz,R}^{(2)}(\omega_2 + \omega_1, \omega_2, \omega_1) \right| e^{i(\varphi_R(\omega_2 + \omega_1, \omega_2, \omega_1))} \right.$$
$$\left. + \chi_{zzz,NR}^{(2)}(\omega_2 + \omega_1, \omega_2, \omega_1) \right\} \left| L_{zz}(\omega_2 + \omega_1) L_{zz}(\omega_2) L_{zz}(\omega_1) \right|$$
$$\times e^{i(\varphi_L(\omega_2 + \omega_1) + \varphi_L(\omega_2) + \varphi_L(\omega_1))} \tag{29}$$

$$\chi_{PPP}^{(2)'}(-\omega_2, -\omega_2 - \omega_1, \omega_1)$$
$$= \frac{1}{A} \left\{ \left| \tilde{\chi}_{zzz,R}^{(2)}(\omega_2 + \omega_1, \omega_2, \omega_1) \right| e^{i(\varphi_R(\omega_2 + \omega_1, \omega_2, \omega_1))} \right.$$
$$\left. + \chi_{zzz,NR}^{(2)}(-\omega_2, -\omega_2 - \omega_1, \omega_1) \right\}$$
$$\times \left| L_{zz}(\omega_2) L_{zz}(\omega_2 + \omega_1) L_{zz}(\omega_1) \right|$$
$$\times e^{i(-\varphi_L(\omega_2 + \omega_1) - \varphi_L(\omega_2) + \varphi_L(\omega_1))} \tag{30}$$

with the (real) scaling factor A accounting for possible differences in field enhancement. The equations show that the resonant and non-resonant contributions ($\tilde{\chi}_{zzz,R}^{(2)}$) and ($\chi_{zzz,NR}^{(2)}$) in Eqs. (29) and (30) are (as expected) phase-shifted in opposite directions by the presence of the local field phases φ_L. Since there is no clear relationship between the intrinsic SFG and DFG responses for the vibrationally non-resonant metal contribution their respective susceptibilities are simply included with the initial frequency arguments. However, due to their vibrationally non-resonant character, these quantities represent (fairly) frequency-independent offsets in the real and imaginary parts that can significantly vary between SFG and DFG spectra.

These offsets are also clearly visible in the data of Fig. 4 and can be approximated by a linear trend.

This slowly-varying nature of $\chi_{zzz,NR}^{(2)}$ can be exploited to determine the phases φ_L using a phase-rotation procedure. Equation (31) shows the difference between the SFG and the rescaled DFG responses [Eqs. (29) and (30)] having rotated their phases by $\pm \varepsilon = \mp(\varphi_L(\omega_2 + \omega_1) + \varphi_L(\omega_2))$. This results in complete cancellation of the resonant features in the difference, with the only surviving term originating from the non-resonant contributions.

$$\chi_{PPP}^{(2)'}(\omega_2 + \omega_1, \omega_2, \omega_1) e^{i\varepsilon} - A\chi_{PPP}^{(2)'}(-\omega_2, -\omega_2 - \omega_1, \omega_1) e^{-i\varepsilon}$$
$$= \left| L_{zz}(\omega_2 + \omega_1) L_{zz}(\omega_2) L_{zz}(\omega_1) \right| \left\{ \chi_{zzz,NR}^{(2)}(\omega_2 + \omega_1, \omega_2, \omega_1) \right.$$
$$\left. - \chi_{zzz,NR}^{(2)}(-\omega_2, -\omega_2 - \omega_1, \omega_1) \right\} e^{i\varphi_L(\omega_1)} \tag{31}$$

The phase rotation (ε) can now be precisely determined by minimising the deviation of this difference spectrum from a straight line as a function of phase rotation and scaling factor A. The result of this procedure is a two-dimensional functional, $P(\varepsilon, A)$ (see "Experimental Section" for details), which should have exactly one minimum. Figure 5 shows an example of this minimisation procedure for the Ag sample. In the top image $P(\varepsilon, A)$ is given as a 2D surface for variable scaling factors (amplitude ratios, A) and phase rotations (ε). As expected, the resulting surface possesses a clear minimum, with values of $\varepsilon = -61.8°$ and $A = 1.34$. The bottom of Fig. 5 then shows the corresponding deviations of the difference spectra from a straight line (accommodating for both the real and imaginary parts) for five different phase rotation values at the optimum amplitude ratio. (It is worth noting that, although for FS, the $\chi_{zzz}^{(2)'}$ component does not dominate to the same extent as for the metals, it can still be treated in the same way, as discussed in the theory section since only the XXZ and ZZZ tensor components are significant.) Whilst fitting the difference spectra to a straight line to account for the non-resonant contributions may seem unnecessary if a background of the non-resonant contributions from clean metal substrates could instead be subtracted, it should be noted that such a background is not trivial to obtain. Firstly, the surface functionalisation of the metals is likely to impact their non-resonant responses, leading to deviations which must be accounted for in the minimisation, thus rendering the background-acquisition moot. Secondly, the rapid oxidation and/or contamination of many metallic substrates under ambient conditions further complicates the situation, likely also yielding deviations in the background. Finally, the ability to extract the phases independently of whether there is a substantial non-resonant background present or not makes for a more widely applicable technique.

The resulting phase values of the high frequency local fields for the five different samples are given in Table II and compared to the calculated phases, also giving their corresponding deviations. The calculations were performed using the three-layer model (3LM, for details see the "Experimental section") which is currently the standard method of estimating the phases of the nonlinear Fresnel factors for such sample systems (thin films atop flat substrates). This model uses refractive index data for the bulk materials from the literature and an approximation of the effective refractive index and thickness of the film as input parameters.[18,28] The data in Table II show a very good match between the measured and theoretical
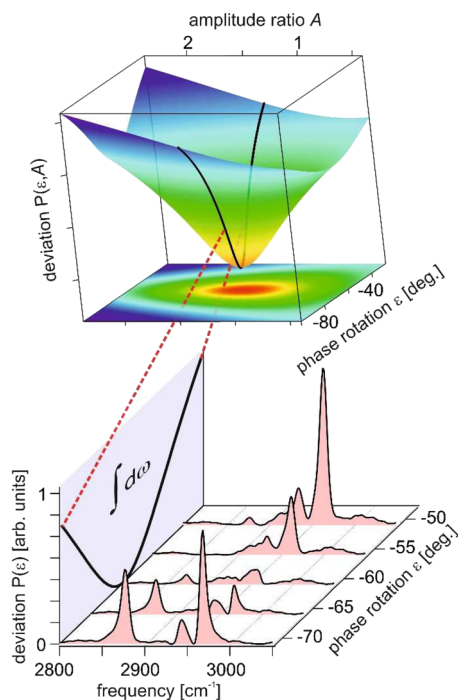
FIG. 5. Depiction of the resulting deviation parameter, $P(\varepsilon, A)$, derived from the minimisation procedure used to obtain the extrinsic phase contribution.

TABLE II. Comparison of the measured local field phase contribution and that calculated from the three-layer model (3LM) using refractive indices from the literature.[1]

Substrate	Measured phase/°	Calculated phase from 3LM/°	Deviation/°
FS	−2.6	0.0	−2.6
Ag	61.8	63.3	−1.5
Pt	44.4	45.2	−0.8
Cu	67.1	69.4	−2.3
Au	67.9	71.0	−3.1

values, with deviations only up to ~3°. This good agreement is on one hand a convincing demonstration of the accuracy of the "Experimental method" but on the other hand this result is also somewhat surprising given the simplicity of the 3LM. It is especially remarkable that, despite the use of bulk values for the refractive indices in the calculation, the 3LM seems to yield a very good approximation of the nonlinear Fresnel factors in such samples. The surface functionalisation of the metal would intuitively be expected to alter the electronic structure of the substrates, and hence also their refractive indices. Nevertheless, the presented results do not show such an effect.

At this point is important to note that there are alternative ways of determining the phase shifts induced by any extrinsic factors. For example, a method which is often implemented in SFG spectroscopy is performing multi-parameter fitting on spectra to fit the resonances.[32] However, there is a substantial qualitative difference between the presented SFG/DFG method and these more commonly used techniques. Multi-parameter fits tend to result in mutual dependencies in their parameters making them susceptible to input bias or misinterpretation, significantly reducing their reliability. In contrast, determination of the extrinsic phases using SFG/DFG in principle requires no fitting. Only in cases where additional (undesired) spectral contributions interfere with the signal of interest (e.g., the metal non-resonant response) does the method require a fitting procedure, but as shown above, this only calls for up to two free parameters (ε and A in the case of the minimisation procedure). Whilst these parameters define the 2D parameter space obtained from the minimisation, it is important to note that the deviations of the difference spectra from a straight line also require four further parameters describing the gradient and intercept for the real and imaginary parts. Nevertheless, these parameters define two independent 2D parameter spaces which are also not linked to the parameter space obtained from the minimisation as they are part of its definition. Therefore, unlike multi-parameter fits, this minimisation procedure avoids significant mutual dependency. Furthermore, as shown in Fig. 5, this fitting procedure also yields a parameter space which is smooth and only contains a single, steep minimum. This removes any potential bias and ensures a highly accurate result.

Having extracted these extrinsic phase contributions, the other described benefit of this methodology can also be demonstrated, namely, obtaining the "true" intrinsic spectra of the molecular samples. The phases in the measured spectra must therefore be back-shifted by the obtained phase values. Figure 6 shows the resulting spectra having implemented this phase-shifting step. The resonant line-shapes of SFG and DFG now show a very good match which clearly indicates that the effect of the high frequency local field phases have successfully been removed. However, on closer inspection of the corresponding SFG and DFG spectra it becomes clear that although the spectral contributions from the vibrational resonances seem identical the overall SFG and DFG spectra also show important differences. For all samples SFG and DFG spectra largely deviate in offset and in case of Cu and Au it can be observed that these offsets even possess deviating curvatures. To understand this discrepancy, it is important to note that the applied correction does not remove the vibrationally non-resonant response but only the phase shifts in the local fields. The spectra therefore still contain a superposition of the intrinsic responses from the molecular monolayer and the metal substrate. As mentioned above, the SFG and DFG responses from the metal surfaces are generally different. In case of Ag and Pt the metal response is only a constant offset. The differences between SFG and DFG responses from those metals therefore only lead to different offsets in the spectra. For the Cu and Au samples, in contrast, the metal response clearly deviates from an offset and even shows deviations from a straight line. This observation is not really surprising as the proximity of the surface plasmon resonance and inter-band transitions to the upconversion frequencies are considerably closer than for Ag and Pt.[33–36] For Cu and Au the metal contributions in the SFG and DFG spectra will consequently not only differ in offset but can obviously also differ in curvature, just as observed in the spectra. It can therefore be concluded that the apparent deviations do not report on inaccuracies in retrieving the intrinsic responses but represent the natural differences in the intrinsic contributions from the metal surface. This interpretation is
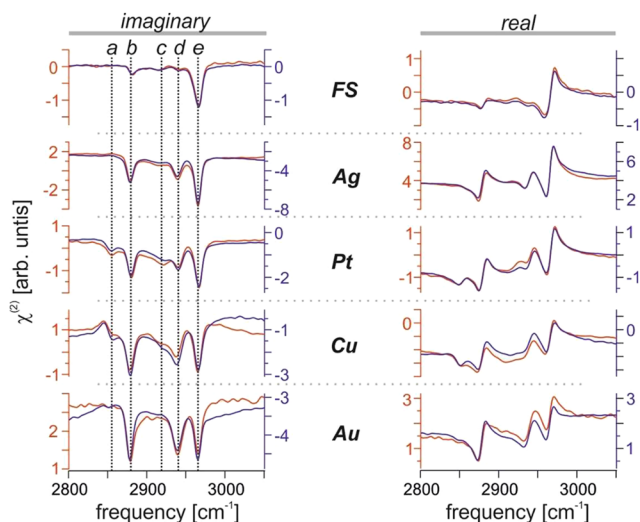
FIG. 6. SFG and DFG spectra for the five monolayer samples after removal of the local field phase effects.

also supported by the fact that the experimentally determined phases of the high frequency Fresnel factors are in close agreement with the theoretical values across all samples.

The next question that must be addressed is to what accuracy the resulting "corrected" spectra reveal the "true" intrinsic spectra of the molecular samples. Equations (29) and (30) show that the spectra will still contain the residual phase shift associated with the IR field $\varphi_L(\omega_1)$ as it contributes equally to SFG and DFG. Nevertheless, for metals in the mid-IR, the phase of L is typically small (on the order of a few degrees[37]) and thus, only represents a minor perturbation. This estimate is also supported by the data presented in Fig. 6. If there were significant phase contributions from $\varphi_L(\omega_1)$ present in the spectra one would expect these to vary for the different metal samples. However, the spectra show that the resonances in all samples are centred at the same frequencies (as shown by the dotted vertical lines), indicating that there are no significant phase-shifts between them. Therefore, although the presented concept cannot completely isolate the intrinsic responses, the phase-corrected spectra represent very good approximations to such.

This gives now the opportunity to further analyse and compare the obtained spectra for the different samples. A closer inspection of the spectra shows that all samples have line-shapes dominated by the same resonant features (indicated by the dotted vertical lines in the imaginary part, labelled "b," "d," and "e"). These frequencies align well with the expected resonances of the terminal CH_3 groups of the SAMs, namely the symmetric ("b") and antisymmetric ("e") C–H stretching modes, as well as the symmetric Fermi resonance ("d"). One strong contrast between the spectra for the metal samples and those from FS are the relative amplitudes of "b" and "d" compared to the "e" resonance (i.e., symmetric to antisymmetric ratio). This is a well-known property of SAMs on dielectrics and originates from the fact that both the XXZ and ZZZ components are significant for these substrate materials.[1] The superposition of these tensor components leads to a large cancellation of the symmetric resonances ("b" and

"d") as observed in the spectra. A further observation from the spectra is the presence of two additional resonant features, particularly for the Pt and Cu samples, labelled "a" and "c," which are assigned to CH_2 stretches (symmetric and anti-symmetric, respectively).[8] A spectrum only containing methyl resonances is characteristic of a perfectly well-packed and defect-free monolayer in an all-trans conformation. By contrast, the appearance of CH_2 signals indicates the presence of gauche defects.[8] The spectra for the different samples show varying amplitudes of the CH_2 signals, which nicely follows the known reactivity of the different metals with thiols. Ag and Au form monolayers with the greatest packing densities whereas Cu and Pt often form more sparsely packed films with greater numbers of defects.[38,39] It is important to note that the presence of gauche defects in the chains will lead to a slight reduction of film thickness and thus potentially a difference in propagation phase between the samples. Nevertheless, this change in thickness will be at most a few Angstroms and give rise to a propagation phase of <1° which can hence be neglected. This example demonstrates how the application of the presented method enables a detailed and unbiased comparison between the different molecular structures formed on such metal samples without the need for any prior assumptions on the details of the intrinsic vibrational spectra such as specific line-shapes models.

CONCLUSIONS AND OUTLOOK

In this contribution, it was shown that crucial aspects of molecular systems like molecular orientation and local dielectric properties are contained within the phase of the measured signal in second order optical experiments. Here, the focus lay firmly on exploiting multiple Liouville pathways to disentangle the measured phase into its constituents. Through a detailed theoretical analysis and confirmatory experiments, it was shown that the resonant phase, intrinsic to the molecular response, can be isolated from extrinsic phase contributions such as any additional propagation of the beams through depth or from absorbing media altering the local field environment. Furthermore, when either of the two aforementioned extrinsic phase contributions are negligible, it is shown that the other can be isolated. This opens the possibility for depth-resolved vibrational studies, as demonstrated in previous work,[16] as well as for the correlation of vibrational spectra with their local field environment, as shown in this work. In addition, it was found in this study that the experimentally determined and the calculated phases of the Fresnel factors showed remarkable similarity, with ≤3° discrepancies. This mutual agreement between the experiment and theory gives significant support to both the experimental methodology and the theoretical model as it is unlikely that both are equally false. This clearly suggests that the three-layer model (3LM) which, despite the lack of experimental validation, is commonly used for such calculations (including in this work) indeed yields accurate values for the nonlinear Fresnel factors, at least for the sample systems used in this study. It will be interesting to investigate whether the observed accuracy is maintained under modified experimental conditions such as applying electric potentials to the metal surface in an electrochemical cell.

In the two simplifying cases discussed above, one of the two extrinsic phase contributions was essentially nullified, allowing the two independent observables (SFG and DFG) to separate the

remaining extrinsic phase from the intrinsic contribution. Although these two cases cover the vast majority of nonlinear vibrational spectroscopy applications, the extension of this concept to systems with even higher complexity can be envisioned. For example, in the electrochemical systems mentioned above both extrinsic phase contributions can be significant, presenting large phase shifts from local fields and substantial depth contributions.[14,40] Provided that the 3LM is found to yield reliable results for the sample system under investigation it is possible to disentangle all three different phase contributions: intrinsic, propagation, and local field. This could be done through separation of the former from the other two and subsequent isolation of the propagation term through subtraction of the calculated local field phase from the 3LM. However, even if the phase contributions from the local field factors cannot be separately determined (calculated), the intrinsic phase can for such samples still be isolated from both extrinsic contributions yielding the undistorted intrinsic vibrational spectrum. This would enable meaningful spectral analysis and comparisons between the vibrationally resonant features from different samples and/or for varying experimental conditions (e.g. different electric potentials). Although, in the context of this work, this aspect is not the main focus, its importance cannot be emphasised enough as the desired molecular information accessible through second order spectroscopy is generally encoded within the details of the resonant line-shapes. It is hence crucial that the intrinsic spectra are correctly obtained.

Overall, the presented method is anticipated to be highly valuable for future interfacial studies with any significant depth dependency or phase contributions from local fields, which describes a substantial range of interfaces spanning many research areas, for example charged liquid interfaces.[41] Finally, it should be noted that the proposed concepts are general and not restricted to the application in second order techniques as shown here. This methodology can readily be extended to higher order spectroscopic methods where even a greater number of different pathways can be probed.

EXPERIMENTAL

SAM formation

Trichloro(octadecyl)silane(OTS) SAMs were prepared following the procedure as described in previous publications.[42,43] 1-Octadecanethiol (ODT) was obtained from Sigma-Aldrich (98% purity) and used as received to form a 5 mM solution in ethanol (96%, Sigma Aldrich, St. Louis, MO, USA) by dissolving with stirring for 20 min. Metal substrates (silver, platinum, copper, and gold) were produced by thermal evaporation on cleaned fused silica windows (Thorlabs, Newton, NJ, USA). The fused silica windows were cleaned following a procedure which involved rinsing and submerging for 15 min in an ultrasonic bath using three different solvents, namely acetone, followed by isopropanol, and finally ultrapure water. The cleaned windows were then dried under a nitrogen stream and used immediately. The SAMs used in this work were formed by submerging the freshly made metal substrate, cleaned by rinsing with ultrapure water (MilliQ, 18.2 MΩ cm) and ethanol (96%, Sigma Aldrich), in the ODT solution for 24 h (Ag and Au), 48 h (Cu), or 60 h (Pt). The substrates were subsequently rinsed with ethanol and were observed to be strongly hydrophobic.

Spectrometer setup

Full details of the experimental setup used for SFG and DFG measurements can be found in Ref. 44. In short, two independent (3 and 4 W) 800 nm outputs (~30 fs, 1 kHz) of a Ti:Sapphire laser (Astrella, Coherent, Santa Clara, CA, US) are used to feed two optical parametric amplifiers (TOPAS, Light Conversion, Vilnius, LT), with one using the generated signal and idler outputs in a DFG unit to generate tuneable mid-IR pulses, and the other being used to generate the signal output which is subsequently frequency-doubled using a BBO crystal to give tuneable upconversion (UC) pulses. These beams are combined in a co-linear geometry and sent to a home-built interferometer which splits the infrared, the first part, combined with the visible UC beam, being used to generate a local oscillator (LO) from quartz and passed through a delay stage to control the timing relative to the second part. The beams are then recombined (IR, UC, and LO) in a co-linear geometry, split in two using an oscillating mirror (500 Hz) to alternate pulses between two paths, going towards a sample and quartz reference, and finally recombined to be sent to the detectors. The combination of a dichroic mirror and polarisation optics allow both the SFG and DFG to be separately measured with balanced detection, each being quasi-simultaneously referenced.

Spectral acquisition and treatment

SFG and DFG spectra were acquired from different experiments using different UC frequencies (800 and 645 nm, respectively). Each spectrum was recorded fully in the time domain by scanning the timing of the LO + UC pulses relative to the IR, ranging from −300 fs to 6000 fs in steps of 0.65 fs to obtain a full interferogram of the vibrational coherence. The resulting spectrum for each sample was obtained by averaging 100 interferograms, performing a Fourier transform (and isolating the positive frequency contribution), and referencing to z-cut quartz.

Phase determination algorithm

The extrinsic phase from the high frequency Fresnel factors was obtained from the SFG and DFG spectra for each substrate using an optimisation algorithm which applied the procedure to calculate the deviation parameter, $P(\varepsilon, A)$, as defined in Eq. (32):

1. Rotate the phase of the complex SFG and DFG spectra in opposite directions by ε.
2. Subtract the DFG spectrum from the SFG spectrum and independently calculate the deviation of the real and imaginary parts from a straight line (obtained through linear regression, labelled $C_{\varepsilon,A}$).
3. Sum the squares of the linear-corrected difference spectra in both the real and imaginary parts.

$$P(\varepsilon, A) = \int d\omega \left| \chi_{SFG}^{(2)} e^{i\varepsilon} - A\chi_{DFG}^{(2)} e^{-i\varepsilon} - C_{\varepsilon,A} \right|^2 \quad (32)$$

Calculation of the Fresnel factors using the three-layer model

A full derivation of the three-layer model (3LM) equations for the local field Fresnel factors can be found elsewhere.[18,28] From this,

the diagonal Fresnel matrix, L, can be given as in Eq. (33) where t and r are the transmission and reflection coefficients defined in Eqs. (34)–(37) for S and P polarised inputs.

$$
L = \begin{bmatrix}
\dfrac{\cos \theta_3}{\cos \theta_1} \dfrac{t_P^{13}\left(1 - r_P^{32} e^{i\delta}\right)}{1 - r_P^{32} r_P^{31} e^{2i\delta}} & 0 & 0 \\[3ex]
0 & \dfrac{t_S^{13}\left(1 + r_S^{32} e^{i\delta}\right)}{1 - r_S^{32} r_S^{31} e^{2i\delta}} & 0 \\[3ex]
0 & 0 & \dfrac{n_1}{n_3} \dfrac{t_P^{13}\left(1 + r_P^{32} e^{i\delta}\right)}{1 - r_P^{32} r_P^{31} e^{2i\delta}}
\end{bmatrix}
\tag{33}
$$

The superscripts on the transmission and reflection coefficients, e.g., 13, are representative of the different media used in the 3LM, with 1 being the incident medium (air), 2 being the bulk substrate (metal or FS), and 3 the thin film (SAM). The other parameters included are δ, the propagation phase obtained through the SAM [given in Eq. (38)], n, the refractive index, and θ_a, representing the beam angle in medium "a" [with relative relations given by Snell's law, Eq. (39)].

$$
r_S^{ab} = \frac{n_a \cos \theta_a - n_b \sin \theta_b}{n_a \cos \theta_a + n_b \sin \theta_b}
\tag{34}
$$

$$
r_P^{ab} = \frac{n_b \cos \theta_a - n_a \sin \theta_b}{n_b \cos \theta_a + n_a \sin \theta_b}
\tag{35}
$$

$$
t_S^{ab} = \frac{2 n_a \cos \theta_a}{n_a \cos \theta_a + n_b \cos \theta_b}
\tag{36}
$$

$$
t_P^{ab} = \frac{2 n_a \cos \theta_a}{n_b \cos \theta_a + n_a \cos \theta_b}
\tag{37}
$$

$$
\delta = k_z^3 h
\tag{38}
$$

$$
n_a \sin \theta_a = n_b \sin \theta_b
\tag{39}
$$

Values used for the calculation of the Fresnel matrix are given in Table III, with the substrate refractive indices (n_2) being sourced from the literature of clean metal substrates.[29–31] The refractive index of the incident medium was taken to be that of air, with a value of unity independent of frequency, and that of the SAM (n_3) to be an effective refractive index of 1.18, representing an average value between the incident medium (air) and the bulk value for ODT (1.46)[45] based on the effective medium approximation.[28] Finally, the propagation phase obtained through the SAM was calculated based on Eq. (38) with a thickness, h, taken to be 2.0 nm, calculated using values for the C–C bond length (1.524 Å) and bond angle (109.5°) based on the VSEPR model for a tetrahedral geometry.[45] Furthermore, the monolayer was taken to be well-packed in an all-trans geometry with a tilt angle of 30° for the purposed of calculation. It should be noted, however, that these approximations may not be representative of the true monolayer structure on each metal (clearly evident, for example, with the presence of gauche defects), but the ultimate phase contribution to the calculated Fresnel factors from

TABLE III. Parameters used for the calculation of the nonlinear Fresnel factors based on the three-layer model.

Parameter	Value
n_{air}	1.00
n_{FS} (645 nm)	1.46
n_{Ag} (645 nm)	0.0534 + 4.37i
n_{Pt} (645 nm)	0.472 + 6.27i
n_{Cu} (645 nm)	0.247 + 3.56i
n_{Au} (645 nm)	0.164 + 3.55i
n_{FS} (800 nm)	1.46
n_{Ag} (800 nm)	0.0368 + 5.57i
n_{Pt} (800 nm)	0.576 + 8.08i
n_{Cu} (800 nm)	0.254 + 5.01i
n_{Au} (800 nm)	0.154 + 4.91i
n_{SAM}	1.23
SAM thickness, h	2.0 nm
θ_a	70°

this thickness are of the order of ~1° and thus these approximations are reasonable for these purposes.

AUTHOR DECLARATIONS

Conflict of Interest

The authors have no conflicts to disclose.

Author Contributions

Alexander P. Fellows: Formal analysis (equal); Methodology (supporting); Validation (equal); Writing – original draft (lead); Writing – review & editing (equal). **Vasileios Balos**: Conceptualization (supporting); Data curation (equal); Formal analysis (equal); Investigation (equal); Methodology (supporting); Validation (equal); Writing – review & editing (equal). **Ben John**: Conceptualization (supporting); Data curation (equal); Formal analysis (equal); Investigation (equal); Methodology (supporting); Writing – review & editing (supporting). **Álvaro Díaz Duque**: Conceptualization (supporting); Formal analysis (equal); Investigation (equal); Methodology (supporting); Writing – review & editing (supporting). **Martin Wolf**: Funding acquisition (equal); Supervision (supporting); Writing – review & editing (supporting). **Martin Thämer**: Conceptualization (lead); Formal analysis (equal); Funding acquisition (equal); Investigation (equal); Methodology (equal); Supervi-

DATA AVAILABILITY

The data presented in this manuscript will be made available by contacting the corresponding author upon reasonable request.

APPENDIX A: LIOUVILLE PATHWAYS FOR SHG AND OR

As described in the main text, the four possible pathways for each light field interaction result in 16 possible pathways for a second order process involving two interactions with the same field. These can be conveniently displayed in a 2D grid format as in Table IV where the individual contribution to the frequency and wavevector of the generated field is indicated by "+" and "−" signs.

If the system is initially in the ground state, which is a reasonable approximation for vibrational spectroscopy, then the 16 potential pathways are reduced to six because stimulated emission cannot occur from the ground state. Of these six pathways, two yield an output field oscillating at twice the input frequency, thus representing second harmonic generation (SHG), and the other four yield a DC field, representing optical rectification (OR) pathways, shown in orange and green in Table IV, respectively.

The total set of 16 contributions can also be seen from the theoretical derivation of the second order polarisation, $P^{(2)}(t)$, in such a case which can be described by Eqs. (A1)–(A6) [where only two interactions at the same frequency, ω, are considered via the introduction of a delta function in Eq. (A2)]

$$P^{(2)}(t) = \varepsilon_0 \int_{-\infty}^{t} dt_1 \int_{-\infty}^{t_1} dt_2\, \chi^{(2)}(t, t_1, t_2)$$
$$: \left(E(t_1) + E^*(t_1)\right)\left(E(t_2) + E^*(t_2)\right) \tag{A1}$$

TABLE IV. Representation of the 16 possible interaction pathways that exist for two interactions with the same field. The "+" and "−" symbols indicate the contribution to the frequency and wavevector of the generated signal field. Highlighted colours are used to indicate the allowed pathways when starting from the ground state, with SHG processes shown in orange and OR in green.

$$= \varepsilon_0 \int_{-\infty}^{\infty} d\omega \int_{-\infty}^{\infty} d\omega' \int_{-\infty}^{t} dt_1 \int_{-\infty}^{t_1} dt_2\, \chi^{(2)}(t, t_1, t_2)$$
$$: \left(E(\omega)e^{-i\omega t_1} + E^*(\omega)e^{i\omega t_1}\right)$$
$$\times \left(E(\omega')e^{-i\omega' t_2} + E^*(\omega')e^{i\omega' t_2}\right)\delta(\omega - \omega') \tag{A2}$$

$$= \varepsilon_0 \int_{-\infty}^{\infty} d\omega \int_{-\infty}^{t} dt_1 \int_{-\infty}^{t_1} dt_2\, \chi^{(2)}(t, t_1, t_2)$$
$$: \left(E(\omega)E(\omega)e^{-i\omega(t_1+t_2)} + E(\omega)E^*(\omega)e^{-i\omega(-t_1+t_2)}\right.$$
$$\left. + E^*(\omega)E(\omega)e^{-i\omega(t_1-t_2)} + E^*(\omega)E^*(\omega)e^{-i\omega(-t_1-t_2)}\right) \tag{A3}$$

$$= \varepsilon_0 \int_{-\infty}^{\infty} d\omega \int_{0}^{\infty} d\tau_1 \int_{0}^{\infty} d\tau_2\, \chi^{(2)}(t, t-\tau_1, t-\tau_1-\tau_2)$$
$$: \left(E(\omega)E(\omega)e^{-i\omega(2t-2\tau_1-\tau_2)}\right.$$
$$+ E(\omega)E^*(\omega)e^{-i\omega(-\tau_2)} + E^*(\omega)E(\omega)e^{-i\omega(\tau_2)}$$
$$\left. + E^*(\omega)E^*(\omega)e^{-i\omega(-2t+2\tau_1+\tau_2)}\right) \tag{A4}$$

$$= \varepsilon_0 \int_{-\infty}^{\infty} d\omega \int_{0}^{\infty} d\tau_1 \int_{0}^{\infty} d\tau_2\, \chi^{(2)}(t, t-\tau_1, t-\tau_1-\tau_2)$$
$$: \left(E(\omega)E(\omega)e^{i\omega(2\tau_1+\tau_2)}e^{-2i\omega t}\right.$$
$$+ E(\omega)E^*(\omega)e^{i\omega\tau_2} + E^*(\omega)E(\omega)e^{-i\omega\tau_2}$$
$$\left. + E^*(\omega)E^*(\omega)e^{-i\omega(2\tau_1+\tau_2)}e^{2i\omega t}\right) \tag{A5}$$

$$= \varepsilon_0 \int_{-\infty}^{\infty} d\omega\, \chi^{(2)}(2\omega, \omega, \omega) : E(\omega)E(\omega)e^{-2i\omega t}$$
$$+ \chi^{(2)}(0, \omega, -\omega) : E(\omega)E^*(\omega)$$
$$+ \chi^{(2)}(0, -\omega, \omega) : E^*(\omega)E(\omega)$$
$$+ \chi^{(2)}(-2\omega, -\omega, -\omega) : E^*(\omega)E^*(\omega)e^{2i\omega t} \tag{A6}$$

where the specific interaction times, t_1 and t_2, are converted to time delays, τ_1 and τ_2, according to Eqs. (A7) and (A8)

$$t_1 = t - \tau_1 \tag{A7}$$
$$t_2 = t - \tau_1 - \tau_2 \tag{A8}$$

After exploiting the Fourier transform definition and evaluation of the time delay integrals, Eq. (A6) clearly shows four contributions (two conjugate pairs) with different $\chi^{(2)}$ terms that are oscillating at either twice the input frequency or not at all, thus indicating the SHG and OR pathways. As this is a second order process, each $\chi^{(2)}$ component will consist of four correlation functions (e.g., the nonlinear polarisation contribution oscillating at $+2\omega$ is contributed to from the four pathways which yield "+" contributions from both interactions, as seen in Table IV) which leads to the 16 possible pathways described in Table IV, as expected. Again, in the ground state, many of these correlation functions will vanish as they represent disallowed pathways.
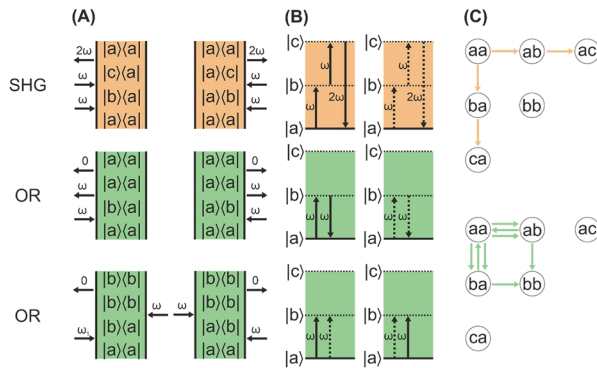
13 November 2023 09:51:36

FIG. 7. Representations of the different pathway contributions to the second order response function when initially in the ground state through two interactions with an electric field oscillating at frequency ω, showing (a) Feynman diagrams, (b) ladder diagrams, and (c) Liouville space pathways.

The specific pathways can also be represented pictographically through Feynman diagrams, ladder (energy level) diagrams, or Liouville space pathways as in Fig. 7 where only the ground state allowed interaction pathways are shown. From these diagrams it is easy to recognise the complex conjugate pairs as they represent mirror images in the Feynman diagrams, inversions of solid and dashed arrows in the ladder diagrams, and reflections along the state population diagonal in the Liouville space pathways. Correspondingly, it is trivial to identify conjugate pairs in Table IV as diagonal boxes within each quadrant. As the conjugate pairs only yield one unique contribution, it is only necessary to measure one of each pair for a full description, thus reducing the effective number of contributions by a factor of two.

APPENDIX B: PERMUTATION SYMMETRY OF $\chi^{(2)}$

If one restricts the contributions to the second order susceptibility to only include those with positive ω_1 (which is easily achieved experimentally), the general expression for $\chi^{(2)}$ includes 32 unique correlation functions. Of these, half will arise from two interactions with the same field (SHG or OR), leaving 16 terms from SFG and DFG (eight each). For SFG, the overall susceptibility is, therefore, given by Eq. (B1).

$$\chi^{(2)}_{ijk}(\omega_2 + \omega_1, \omega_2, \omega_1)$$

$$= \frac{N}{2\varepsilon_0\hbar^2} \sum_{pqr} \rho^{(0)}_{pp} \left\{ \frac{\mu^i_{pr}\mu^j_{rq}\mu^k_{qp}}{(\omega_1 - \omega_{qp} + i\Gamma_{qp})(\omega_2 + \omega_1 - \omega_{rp} + i\Gamma_{rp})} \right. \tag{B1a}$$

$$- \frac{\mu^i_{rq}\mu^j_{rp}\mu^k_{qp}}{(\omega_1 - \omega_{qp} + i\Gamma_{qp})(\omega_2 + \omega_1 - \omega_{qr} + i\Gamma_{qr})} \tag{B1b}$$

$$- \frac{\mu^i_{qr}\mu^j_{rp}\mu^k_{pq}}{(\omega_1 - \omega_{pq} + i\Gamma_{pq})(\omega_2 + \omega_1 - \omega_{rq} + i\Gamma_{rq})} \tag{B1c}$$

$$+ \frac{\mu^i_{rp}\mu^j_{qr}\mu^k_{pq}}{(\omega_1 - \omega_{pq} + i\Gamma_{pq})(\omega_2 + \omega_1 - \omega_{pr} + i\Gamma_{pr})} \tag{B1d}$$

$$+ \frac{\mu^i_{pr}\mu^j_{qp}\mu^k_{rq}}{(\omega_2 - \omega_{qp} + i\Gamma_{qp})(\omega_2 + \omega_1 - \omega_{rp} + i\Gamma_{rp})} \tag{B1e}$$

$$- \frac{\mu^i_{rq}\mu^j_{qp}\mu^k_{pr}}{(\omega_2 - \omega_{qp} + i\Gamma_{qp})(\omega_2 + \omega_1 - \omega_{qr} + i\Gamma_{qr})} \tag{B1f}$$

$$- \frac{\mu^i_{qr}\mu^j_{pq}\mu^k_{rp}}{(\omega_2 - \omega_{pq} + i\Gamma_{pq})(\omega_2 + \omega_1 - \omega_{rq} + i\Gamma_{rq})} \tag{B1g}$$

$$+ \frac{\mu^i_{rp}\mu^j_{pq}\mu^k_{qr}}{(\omega_2 - \omega_{pq} + i\Gamma_{pq})(\omega_2 + \omega_1 - \omega_{pr} + i\Gamma_{pr})} \left. \right\} \tag{B1h}$$

By rearrangement of the transition dipole moments in the numerators for each correlation function, it can be noticed that every term expresses a progression of three pairs of indices that have the form: $pa \rightarrow ab \rightarrow bp$ where "a" and "b" can be either "q" or "r" in the summation. As "q" and "r" are completely free parameters in each term [(but "p" is not due to the multiplication of every term by the density of states for state "p" ($\rho^{(0)}_{pp}$)], they can be interchanged without loss of generality. This, therefore, leaves eight permutations of the form $pr \rightarrow rq \rightarrow qp$, where the only distinction in the numerators comes from the order of indices i, j, k, representing which field is associated with the specific transition. Since there are six possible permutations of i, j, k there must be repetitions, and indeed it is possible to see (with appropriate swapping of "q" and "r") that term (B1b) has the same numerator as term (B1g), and term (B1c) has the same as term (B1f). Taking terms (B1b) and (B1g) then, for example, it is possible to combine them (swapping "q" and "r" in the latter) as in Eq. (B2).

$$- \frac{\mu^i_{rq}\mu^j_{pr}\mu^k_{qp}}{(\omega_1 - \omega_{qp} + i\Gamma_{qp})(\omega_2 + \omega_1 - \omega_{qr} + i\Gamma_{qr})}$$

$$- \frac{\mu^i_{rq}\mu^j_{pr}\mu^k_{qp}}{(\omega_2 - \omega_{pr} + i\Gamma_{pr})(\omega_2 + \omega_1 - \omega_{qr} + i\Gamma_{qr})}$$

$$= - \frac{\mu^i_{rq}\mu^j_{pr}\mu^k_{qp}}{(\omega_2 + \omega_1 - \omega_{qr} + i\Gamma_{qr})} \left\{ \frac{1}{(\omega_1 - \omega_{qp} + i\Gamma_{qp})} \right.$$

$$\left. + \frac{1}{(\omega_2 - \omega_{pr} + i\Gamma_{pr})} \right\} \tag{B2a}$$

$$= - \frac{\mu^i_{rq}\mu^j_{pr}\mu^k_{qp}}{(\omega_2 + \omega_1 - \omega_{qr} + i\Gamma_{qr})} \left\{ \frac{\omega_2 + \omega_1 - \omega_{qr} + i(\Gamma_{pr} + \Gamma_{qp})}{(\omega_1 - \omega_{qp} + i\Gamma_{qp})(\omega_2 - \omega_{pr} + i\Gamma_{pr})} \right\} \tag{B2b}$$

$$= - \frac{\mu^i_{rq}\mu^j_{pr}\mu^k_{qp}}{(\omega_1 - \omega_{qp} + i\Gamma_{qp})(\omega_2 - \omega_{pr} + i\Gamma_{pr})}$$

$$\times \left\{ \frac{\omega_2 + \omega_1 - \omega_{qr} + i(\Gamma_{pr} + \Gamma_{qp})}{\omega_2 + \omega_1 - \omega_{qr} + i\Gamma_{qr}} \right\} \tag{B2c}$$

Similarly, terms (B1c) and (B1f) can be combined into the single term as in Eq. (B3).

$$- \frac{\mu_{rq}^i \mu_{qp}^j \mu_{pr}^k}{(\omega_1 - \omega_{pr} + i\Gamma_{pr})(\omega_2 + \omega_1 - \omega_{qr} + i\Gamma_{qr})}$$

$$- \frac{\mu_{rq}^i \mu_{qp}^j \mu_{pr}^k}{(\omega_2 - \omega_{qp} + i\Gamma_{qp})(\omega_2 + \omega_1 - \omega_{qr} + i\Gamma_{qr})}$$

$$= - \frac{\mu_{rq}^i \mu_{qp}^j \mu_{pr}^k}{(\omega_1 - \omega_{pr} + i\Gamma_{pr})(\omega_2 - \omega_{qp} + i\Gamma_{qp})}$$

$$\times \left\{ \frac{\omega_2 + \omega_1 - \omega_{qr} + i(\Gamma_{pr} + \Gamma_{qp})}{\omega_2 + \omega_1 - \omega_{qr} + i\Gamma_{qr}} \right\} \tag{B3}$$

Therefore, by substituting these expressions into Eq. (B1) along with an appropriate swapping of "q" and "r" in specific correlation functions, the second order susceptibility for SFG with positive ω_1 can be written as in Eq. (B4).

$$\chi_{ijk}^{(2)}(\omega_2 + \omega_1, \omega_2, \omega_1)$$

$$= \frac{N}{2\varepsilon_0 \hbar^2} \sum_{pqr} \rho_{pp}^{(0)} \left\{ \frac{\mu_{pr}^i \mu_{rq}^j \mu_{qp}^k}{(\omega_1 - \omega_{qp} + i\Gamma_{qp})(\omega_2 + \omega_1 - \omega_{rp} + i\Gamma_{rp})} \right. \tag{B4a}$$

$$+ \frac{\mu_{qp}^i \mu_{rq}^j \mu_{pr}^k}{(\omega_1 - \omega_{pr} + i\Gamma_{pr})(\omega_2 + \omega_1 - \omega_{pq} + i\Gamma_{pq})} \tag{B4b}$$

$$- \frac{\mu_{rq}^i \mu_{pr}^j \mu_{qp}^k}{(\omega_1 - \omega_{qp} + i\Gamma_{qp})(\omega_2 - \omega_{pr} + i\Gamma_{pr})}$$

$$\times \left\{ \frac{\omega_2 + \omega_1 - \omega_{qr} + i(\Gamma_{pr} + \Gamma_{qp})}{\omega_2 + \omega_1 - \omega_{qr} + i\Gamma_{qr}} \right\} \tag{B4c}$$

$$- \frac{\mu_{rq}^i \mu_{qp}^j \mu_{pr}^k}{(\omega_1 - \omega_{pr} + i\Gamma_{pr})(\omega_2 - \omega_{qp} + i\Gamma_{qp})}$$

$$\times \left\{ \frac{\omega_2 + \omega_1 - \omega_{qr} + i(\Gamma_{pr} + \Gamma_{qp})}{\omega_2 + \omega_1 - \omega_{qr} + i\Gamma_{qr}} \right\} \tag{B4d}$$

$$+ \frac{\mu_{pr}^i \mu_{qp}^j \mu_{rq}^k}{(\omega_2 - \omega_{qp} + i\Gamma_{qp})(\omega_2 + \omega_1 - \omega_{rp} + i\Gamma_{rp})} \tag{B4e}$$

$$+ \left. \frac{\mu_{qp}^i \mu_{pr}^j \mu_{rq}^k}{(\omega_2 - \omega_{pr} + i\Gamma_{pr})(\omega_2 + \omega_1 - \omega_{pq} + i\Gamma_{pq})} \right\} \tag{B4f}$$

By swapping frequencies $\omega_2 + \omega_1$ and ω_2 with negation, along with their corresponding indices, results in the expression for the second order susceptibility in Eq. (B5).

$$\chi_{jik}^{(2)}(-\omega_2, -\omega_2 - \omega_1, \omega_1)$$

$$= \frac{N}{2\varepsilon_0 \hbar^2} \sum_{pqr} \rho_{pp}^{(0)} \left\{ \frac{\mu_{pr}^j \mu_{rq}^i \mu_{qp}^k}{(\omega_1 - \omega_{qp} + i\Gamma_{qp})(-\omega_2 - \omega_{rp} + i\Gamma_{rp})} \right. \tag{B5a}$$

$$+ \frac{\mu_{qp}^j \mu_{rq}^i \mu_{pr}^k}{(\omega_1 - \omega_{pr} + i\Gamma_{pr})(-\omega_2 - \omega_{pq} + i\Gamma_{pq})} \tag{B5b}$$

$$- \frac{\mu_{rq}^j \mu_{pr}^i \mu_{qp}^k}{(\omega_1 - \omega_{qp} + i\Gamma_{qp})(-\omega_2 - \omega_1 - \omega_{pr} + i\Gamma_{pr})}$$

$$\times \left\{ \frac{-\omega_2 - \omega_{qr} + i(\Gamma_{pr} + \Gamma_{qp})}{-\omega_2 - \omega_{qr} + i\Gamma_{qr}} \right\} \tag{B5c}$$

$$- \frac{\mu_{rq}^j \mu_{qp}^i \mu_{pr}^k}{(\omega_1 - \omega_{pr} + i\Gamma_{pr})(-\omega_2 - \omega_1 - \omega_{qp} + i\Gamma_{qp})}$$

$$\times \left\{ \frac{-\omega_2 - \omega_{qr} + i(\Gamma_{pr} + \Gamma_{qp})}{-\omega_2 - \omega_{qr} + i\Gamma_{qr}} \right\} \tag{B5d}$$

$$+ \frac{\mu_{pr}^j \mu_{qp}^i \mu_{rq}^k}{(-\omega_2 - \omega_1 - \omega_{qp} + i\Gamma_{qp})(-\omega_2 - \omega_{rp} + i\Gamma_{rp})} \tag{B5e}$$

$$+ \left. \frac{\mu_{qp}^j \mu_{pr}^i \mu_{rq}^k}{(-\omega_2 - \omega_1 - \omega_{pr} + i\Gamma_{pr})(-\omega_2 - \omega_{pq} + i\Gamma_{pq})} \right\} \tag{B5f}$$

Therefore, by manipulating the signs, this can be rewritten as in Eq. (B6).

$$\chi_{jik}^{(2)}(-\omega_2, -\omega_2 - \omega_1, \omega_1)$$

$$= \frac{N}{2\varepsilon_0 \hbar^2} \sum_{pqr} \rho_{pp}^{(0)} \left\{ - \frac{\mu_{pr}^j \mu_{rq}^i \mu_{qp}^k}{(\omega_1 - \omega_{qp} + i\Gamma_{qp})(\omega_2 - \omega_{pr} - i\Gamma_{pr})} \right. \tag{B6a}$$

$$- \frac{\mu_{qp}^j \mu_{rq}^i \mu_{pr}^k}{(\omega_1 - \omega_{pr} + i\Gamma_{pr})(\omega_2 - \omega_{qp} - i\Gamma_{qp})} \tag{B6b}$$

$$+ \frac{\mu_{rq}^j \mu_{pr}^i \mu_{qp}^k}{(\omega_1 - \omega_{qp} + i\Gamma_{qp})(\omega_2 + \omega_1 - \omega_{rp} - i\Gamma_{rp})}$$

$$\times \left\{ \frac{\omega_2 - \omega_{rq} - i(\Gamma_{rp} + \Gamma_{qp})}{\omega_2 - \omega_{rq} - i\Gamma_{rq}} \right\} \tag{B6c}$$

$$+ \frac{\mu_{rq}^j \mu_{qp}^i \mu_{pr}^k}{(\omega_1 - \omega_{pr} + i\Gamma_{pr})(\omega_2 + \omega_1 - \omega_{pq} - i\Gamma_{qp})}$$

$$\times \left\{ \frac{\omega_2 - \omega_{rq} - i(\Gamma_{rp} + \Gamma_{qp})}{\omega_2 - \omega_{rq} - i\Gamma_{qr}} \right\} \tag{B6d}$$

$$+ \frac{\mu_{pr}^j \mu_{qp}^i \mu_{rq}^k}{(\omega_2 + \omega_1 - \omega_{pq} - i\Gamma_{pq})(\omega_2 - \omega_{pr} - i\Gamma_{pr})} \tag{B6e}$$

$$+ \left. \frac{\mu_{qp}^j \mu_{pr}^i \mu_{rq}^k}{(\omega_2 + \omega_1 - \omega_{rp} - i\Gamma_{pr})(\omega_2 - \omega_{qp} - i\Gamma_{qp})} \right\} \tag{B6f}$$

TABLE V. Corresponding contributions to the SFG and DFG susceptibility on the assumption of non-resonant $\omega_2 + \omega_1$ and ω_2 interactions.

Term in SFG [Eq. (B4)]	Term in DFG [Eq. (B6)]
(B4a)	(B6c)
(B4b)	(B6d)
(B4c)	(B6a)
(B4d)	(B6b)
(B4e)	(B6f)
(B4f)	(B6e)

In the case of both $\omega_2 + \omega_1$ and ω_2 being off-resonant, a direct comparison can hence be made between the terms in Eq. (B6) with those in Eq. (B4). Specifically, the specific terms correspond exactly to each other as in Table V.

REFERENCES

[1] H. F. Wang, W. Gan, R. Lu, Y. Rao, and B. H. Wu, "Quantitative spectral and orientational analysis in surface sum frequency generation vibrational spectroscopy (SFG-VS)," Int. Rev. Phys. Chem. **24**(2), 191–256 (2005).

[2] C. S. Tian and Y. R. Shen, "Recent progress on sum-frequency spectroscopy," Surf. Sci. Rep. **69**(2–3), 105–131 (2014).

[3] L. Fu, Z. Wang, and E. C. Y. Yan, "Chiral vibrational structures of proteins at interfaces probed by sum frequency generation spectroscopy," Int. J. Mol. Sci. **12**(12), 9404–9425 (2011).

[4] Y. R. Shen, "Revisiting the basic theory of sum-frequency generation," J. Chem. Phys. **153**, 180901 (2020).

[5] Z. Chen, Y. R. Shen, and G. A. Somorjai, "Studies of polymer surfaces by sum frequency generation vibrational spectroscopy," Annu. Rev. Phys. Chem. **53**(1), 437–465 (2002).

[6] F. Vidal and A. Tadjeddine, "Sum-frequency generation spectroscopy of interfaces," Rep. Prog. Phys. **68**(5), 1095–1127 (2005).

[7] G. L. Richmond, "Molecular bonding and interactions at aqueous surfaces as probed by vibrational sum frequency spectroscopy," Chem. Rev. **102**(8), 2693–2724 (2002).

[8] A. G. Lambert, P. B. Davies, and D. J. Neivandt, "Implementing the theory of sum frequency generation vibrational spectroscopy: A tutorial review," Appl. Spectrosc. Rev. **40**(2), 103–145 (2005).

[9] Y. R. Shen, *Fundamentals of Sum-Frequency Spectroscopy* (Cambridge University Press, Cambridge, 2016).

[10] Y. Tong, Y. Zhao, N. Li, M. Osawa, P. B. Davies, and S. Ye, "Interference effects in the sum frequency generation spectra of thin organic films. I. Theoretical modeling and simulation," J. Chem. Phys. **133**(3), 034704 (2010).

[11] G. Gonella, C. Lütgebaucks, A. G. F. De Beer, and S. Roke, "Second harmonic and sum-frequency generation from aqueous interfaces is modulated by interference," J. Phys. Chem. C **120**(17), 9165–9173 (2016).

[12] L. Wang, S. Nihonyanagi, K. I. Inoue, K. Nishikawa, A. Morita, S. Ye, and T. Tahara, "Effect of frequency-dependent fresnel factor on the vibrational sum frequency generation spectra for liquid/solid interfaces," J. Phys. Chem. C **123**(25), 15665–15673 (2019).

[13] L. Dreesen, C. Humbert, M. Celebi, J. J. Lemaire, A. A. Mani, P. A. Thiry, and A. Peremans, "Influence of the metal electronic properties on the sum-frequency generation spectra of dodecanethiol self-assembled monolayers on Pt(111), Ag(111) and Au(111) single crystals," Appl. Phys. B **74**(7–8), 621–625 (2002).

[14] G. Zwaschka, M. Wolf, R. K. Campen, and Y. Tong, "A microscopic model of the electrochemical vibrational Stark effect: Understanding VSF spectroscopy of (bi)sulfate on Pt(111)," Surf. Sci. **678**, 78–85 (2018).

[15] E. H. G. Backus, N. Garcia-Araez, M. Bonn, and H. J. Bakker, "On the role of fresnel factors in sum-frequency generation spectroscopy of metal-water and metal-oxide-water interfaces," J. Phys. Chem. C **116**(44), 23351–23361 (2012).

[16] V. Balos, T. Garling, A. D. Duque, B. John, M. Wolf, and M. Thämer, "Phase-sensitive vibrational sum and difference frequency-generation spectroscopy enabling nanometer-depth profiling at interfaces," J. Phys. Chem. C **126**(26), 10818–10832 (2022).

[17] R. W. Boyd, *Nonlinear Optics*, 3rd ed. (Academic Press, Rochester, New York, 2008).

[18] A. Morita, *Theory of Sum Frequency Generation Spectroscopy* (Springer Nature Singapore, Singapore, 2018).

[19] Y.-R. Shen, *Principles of Nonlinear Optics* (Wiley-Interscience, New York, 1984).

[20] Y. Shen, "Optical second harmonic generation at interfaces," Annu. Rev. Phys. Chem. **40**(1), 327–350 (1989).

[21] P. A. Franken, A. E. Hill, C. W. Peters, and G. Weinreich, "Generation of optical harmonics," Phys. Rev. Lett. **7**(4), 118–119 (1961).

[22] M. Bass, P. A. Franken, J. F. Ward, and G. Weinreich, "Optical rectification," Phys. Rev. Lett. **9**(11), 446–448 (1962).

[23] X. Wei, S. C. Hong, X. Zhuang, T. Goto, and Y. R. Shen, "Nonlinear optical studies of liquid crystal alignment on a rubbed polyvinyl alcohol surface," Phys. Rev. E **62**(4), 5160–5172 (2000).

[24] A. Lagutchev, S. A. Hambir, and D. D. Dlott, "Nonresonant background suppression in broadband vibrational sum-frequency generation spectroscopy," J. Phys. Chem. C **111**(37), 13645–13647 (2007).

[25] H. Yui, Y. Hirose, and T. Sawada, "New approaches to liquid interfaces through changes in the refractive index and nonlinear susceptibility utilizing ultrashort laser pulses," Anal. Sci. **20**(11), 1493–1499 (2004).

[26] O. Pluchery, C. Humbert, M. Valamanesh, E. Lacaze, and B. Busson, "Enhanced detection of thiophenol adsorbed on gold nanoparticles by SFG and DFG nonlinear optical spectroscopy," Phys. Chem. Chem. Phys. **11**(35), 7729–7737 (2009).

[27] D. A. Genov, A. K. Sarychev, V. M. Shalaev, and A. Wei, "Resonant field enhancements from metal nanoparticle arrays," Nano Lett. **4**(1), 153–158 (2004).

[28] G. J. Simpson, *Nonlinear Optical Polarization Analysis in Chemistry and Biology* (Cambridge University Press, Cambridge, 2017).

[29] P. B. Johnson and R. W. Christy, "Optical constants of the noble metals," Phys. Rev. B **6**(12), 4370–4379 (1972).

[30] W. S. M. Werner, K. Glantschnig, and C. Ambrosch-Draxl, "Optical constants and inelastic electron-scattering data for 17 elemental metals," J. Phys. Chem. Ref. Data **38**(4), 1013–1092 (2009).

[31] L. V. Rodríguez-de Marcos, J. I. Larruquert, J. A. Méndez, and J. A. Aznárez, "Self-consistent optical constants of SiO$_2$ and Ta$_2$O$_5$ films," Opt. Mater. Express **6**(11), 3622 (2016).

[32] B. Busson and A. Tadjeddine, "Non-uniqueness of parameters extracted from resonant second-order nonlinear optical spectroscopies," J. Phys. Chem. C **113**(52), 21895–21902 (2009).

[33] K. K. R. Datta, M. Eswaramoorthy, and C. N. R. Rao, "Water-solubilized aminoclay-metal nanoparticle composites and their novel properties," J. Mater. Chem. **17**(7), 613–615 (2007).

[34] D. O. Shin, J. R. Jeong, T. H. Han, C. M. Koo, H. J. Park, Y. T. Lim, and S. O. Kim, "A plasmonic biosensor array by block copolymer lithography," J. Mater. Chem. **20**(34), 7241–7247 (2010).

[35] V. Amendola and M. Meneghetti, "Laser ablation synthesis in solution and size manipulation of noble metal nanoparticles," Phys. Chem. Chem. Phys. **11**(20), 3805–3821 (2009).

[36] S. Peiris, J. McMurtrie, and H. Y. Zhu, "Metal nanoparticle photocatalysts: Emerging processes for green organic synthesis," Catal. Sci. Technol. **6**(2), 320–338 (2016).

[37] S. Adachi, *The Handbook on Optical Constants of Metals: In Tables and Figures* (World Scientific Publishing Co., Singapore, 2012).

[38] P. E. Laibinis, G. M. Whitesides, D. L. Allara, Y. T. Tao, A. N. Parikh, and R. G. Nuzzo, "Comparison of the structures and wetting properties of self-assembled monolayers of n-alkanethiols on the coinage metal surfaces, copper, silver, and gold," J. Am. Chem. Soc. **113**(19), 7152–7167 (1991).

[39] Z. Li, S. C. Chang, and R. S. Williams, "Self-assembly of alkanethiol molecules onto platinum and platinum oxide surfaces," Langmuir **19**(17), 6744–6749 (2003).

[40] F. M. Geiger, "Second harmonic generation, sum frequency generation, and $\chi^{(3)}$: Dissecting environmental interfaces with a nonlinear optical Swiss army knife," Annu. Rev. Phys. Chem. **60**, 61–83 (2009).

[41] G. Gonella, E. H. G. Backus, Y. Nagata, D. J. Bonthuis, P. Loche, A. Schlaich, R. R. Netz, A. Kühnle, I. T. McCrum, M. T. M. Koper, M. Wolf, B. Winter, G. Meijer, R. K. Campen, and M. Bonn, "Water at charged interfaces," Nat. Rev. Chem **5**(7), 466–485 (2021).

[42] S. P. Pujari, L. Scheres, A. T. M. Marcelis, and H. Zuilhof, "Covalent surface modification of oxide surfaces," Angew. Chem., Int. Ed. **53**(25), 6322–6356 (2014).

[43] H.-G. Steinrück, "Structure of self-assembled and surface-frozen monolayers of n-silanes, porphyrins and alcohols on metal oxides," Dr. rer. nat. thesis, Friedrich-Alexander-Universität Erlangen-Nürnberg, 2015.

[44] M. Thämer, R. K. Campen, and M. Wolf, "Detecting weak signals from interfaces by high accuracy phase-resolved SFG spectroscopy," Phys. Chem. Chem. Phys. **20**(40), 25875–25882 (2018).

[45] *CRC Handbook of Chemistry and Physics*, 95th ed., edited by D. R. Lide (CRC Press, Boca Raton, Florida, 2004), Sec.3, Physical Constants of Organic Compounds.

13 November 2023 09:51:36